Received 23 August, 2024; revised 22 January, 2025; accepted XX Month, XXXX; Date of publication XX Month, XXXX; date of current version 31 March, 2025.

Digital Object Identifier 10.1109/TMLCN.2025.1234567

DoNext: An Open-Access Measurement Dataset for Machine Learning-Driven 5G Mobile Network Analysis

Hendrik Schippers, Melina Geis, Stefan Böcker, and Christian Wietfeld

[1]Communication Networks Institute (CNI), TU Dortmund University, Otto-Hahn-Str. 6, 44227 Dortmund, NRW, Germany

Corresponding author: Hendrik Schippers (email: hendrik.schippers@tu-dortmund.de).

This work has been supported by the Federal Ministry of Education and Research (BMBF) in the course of the 6GEM Research Hub under grant number 16KISK038, the German Federal Ministry for Digital and Transport (BMDV) in the context of the project Virtual Integration of decentralized charging infrastructure in cab stands under the funding reference 16DKVM006B, and by the Ministry of Economic Affairs, Industry, Climate Action and Energy of the state of North Rhine–Westphalia (MWIKE NRW) along with the Competence Center 5G.NRW under grant number 005–01903–0047.

ABSTRACT Future mobile use cases such as teleoperation rely on highly available mobile networks. Due to the nature of the mobile access channel and the inherent competition, the availability may be restricted in certain initially unknown areas or timespans. We automated mobile network data acquisition using a smartphone application and dedicated hardware to address this challenge, providing detailed connectivity insights. DoNext, a massive dataset of 4G and 5G mobile network data and active measurements, was collected over two years in Dortmund, Germany. To the best of our knowledge, it is the most extensive openly available mobile dataset. Machine learning methods were applied to the data to demonstrate its utility in key performance indicator prediction. Radio environmental maps facilitating key performance indicator predictions and application planning across different locations are generated through spatial aggregation for in-advance predictions. We also showcase signal strength modeling with transfer learning for arbitrary locations in individual mobile network cells, covering private and restricted areas. By openly providing the dataset, we aim to enable other researchers to develop and evaluate their machine-learning methods without conducting extensive measurement campaigns.

INDEX TERMS 5G new radio, 6G, dataset, machine learning, predictive QoS, multi-MNO, channel modelling, transfer learning.

Dataset available on https://tiny.cc/DoNext

I. Introduction

Mobile networks are increasingly important for users, while applications are becoming more demanding and critical. Examples are smart city applications, Vehicle to Everything (V2X) and Intelligent Transportation Systems (ITSs) that require certain service guarantees. Devices range from connected smart sensors to Connected and Automated Vehicles (CAVs) supporting teleoperation. While some applications may be stationary, pre-deployment conformance testing is particularly difficult for mobile use cases. In addition to the variable location, mobile network utilization tends to vary, and network enhancements are applied over time. As a result, heterogeneous, full-coverage data and sophisticated Machine Learning (ML) are required for deployment planning and feasibility.

Over a decade ago, the minimization of drive tests leveraging user data was discussed [1]. Still, spatially and temporally detailed connectivity data remains scarce. Therefore, in this work, we aim to fill this gap and present DoNext, our comprehensive dataset of mobile network measurements along with ML-based analysis, and prediction of relevant Key Performance Indicators (KPIs). With the help of a previously developed and improved measurement application [2], data from multiple measurement devices is aggregated, analyzed and visualized. Providing users with insights into data and ML methods is solved via a digital mobile network twin interface, which can be interconnected with twins of other domains (e.g., mobile network-aware trajectory selection for teleoperation). In this way, the dataset can be leveraged for in-advance planning and live interaction with already

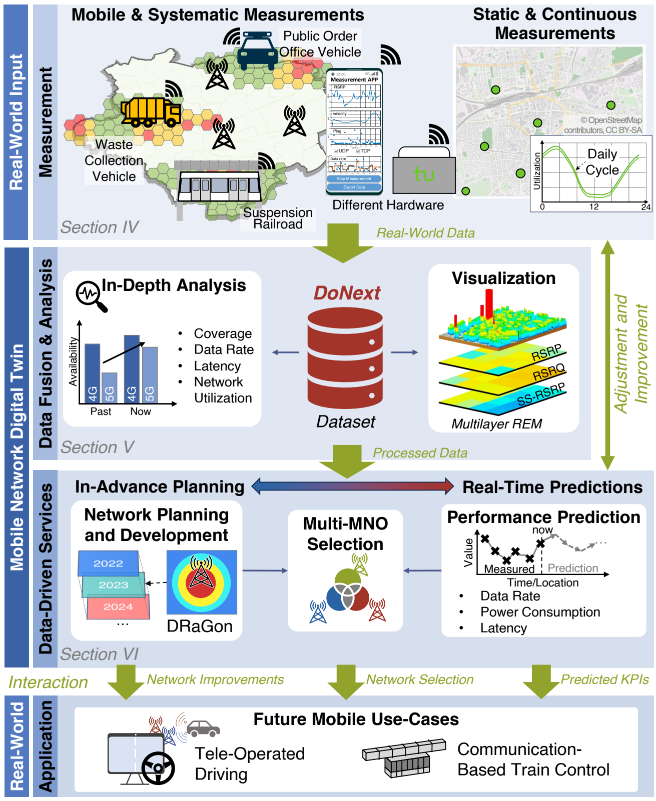

FIGURE 1: Vision of the proposed *DoNext* dataset benefiting future mobile use-cases and mobile network extension.

deployed applications, as shown in Fig. 1. By repeatedly updating prediction and planning models as new data becomes available, provided services can be improved.

Due to its unique properties, we call our dataset *DoNext*. While the data originates in Dortmund (DO), it can be leveraged to *do* sophisticated analysis. Furthermore, it showcases possible *next* steps in mobile networking applications. Finally, *x* stands for the multiple network technologies and operators that are included [3]. *DoNext* is the most comprehensive publicly available dataset of its kind, offering a combination of active and passive measurements across diverse environments and is designed for ML-driven analysis.

Our contributions are summarized as follows:

- Discussing and comparing public datasets of mobile network measurement campaigns and systems.
- Introducing an automated mobile network data acquisition system providing services derived on this basis in the context of a mobile network digital twin.
- We present DoNext, a comprehensive dataset of 4G and 5G measurements in the area of Dortmund, Germany, consisting of passive and active measurements over almost two years.
- In-depth data analysis and ML methods are applied to the dataset, underscoring its relevance.
- Showcasing the usability of the dataset in predictive Quality of Service (QoS), radio propagation modeling and multi-Mobile Network Operator (MNO) use cases.

The remainder of the article is structured as follows. After discussing the related work in Sec. II, an overview of relevant ML methods and mobile network aspects is given in Sec. III. Afterwards, our approach to generating a massive dataset of mobile network connectivity data of Dortmund is presented in Sec. IV. Finally, detailed results and analysis of the achieved KPIs are provided in Sec. V, along with detailed ML-based analysis of the data in Sec. VI.

II. Measurement Campaigns and Methodologies for Mobile Network KPI Tracking

Understanding the limitations of existing datasets and tools is essential for contextualizing the contribution of DoNext. Here, we compare our dataset with publicly available alternatives and evaluate existing measurement applications.

A. Public Mobile Network Measurement Datasets

To cope with their requirements, several previous works have conducted some kind of mobile network measurements. However, the measurement setups used vary greatly depending on the purpose and application of the data. Some studies only measured passive reference signals; others performed only static measurements. For example, the authors of [15] performed latency measurements and prediction on a vehicular dataset. Other works evaluated data rate prediction methods on their own datasets [16–18]. These were partially conducted in private Long Term Evolution (LTE) networks. Due to less competition, results might not be directly comparable to public networks. However, the previously listed works did not publish their measured data, which is why they are omitted from the comparison in Tab. I.

While we only consider openly available datasets published in the context of peer-reviewed publications, there are also various datasets on online platforms [19, 20] of varying quality, quantity and scope. We also do not consider cabled measurements [21] as well as simulated data, such as [22]. The listed works in Tab. I span multiple generations of mobile technologies. While primarily, the older publications only cover 4G networks [4, 9, 14], in recent years, 5G Non-Standalone (NSA) and partly Standalone (SA) networks were introduced. Measurement campaigns also vary in their environmental focus. While urban environments are the most common [6, 7, 11], some studies also extended their scope to include other scenarios [4, 8, 9, 12, 14]. Most of the studies deployed smartphone-based measurement applications. While these have the advantage of high scalability in addition to capturing the real behavior of common smartphone users, dedicated modems and proprietary measurement devices can potentially capture more metrics in a higher resolution. However, two of three campaigns deploying proprietary devices lack data rate measurements (cf. Tab. I). These are highly dependent on the direction and the used protocol configuration. While Transmission Control Protocol (TCP)-based measurements are influenced by congestion control and slow-start phenomenons, which may reduce the achieved

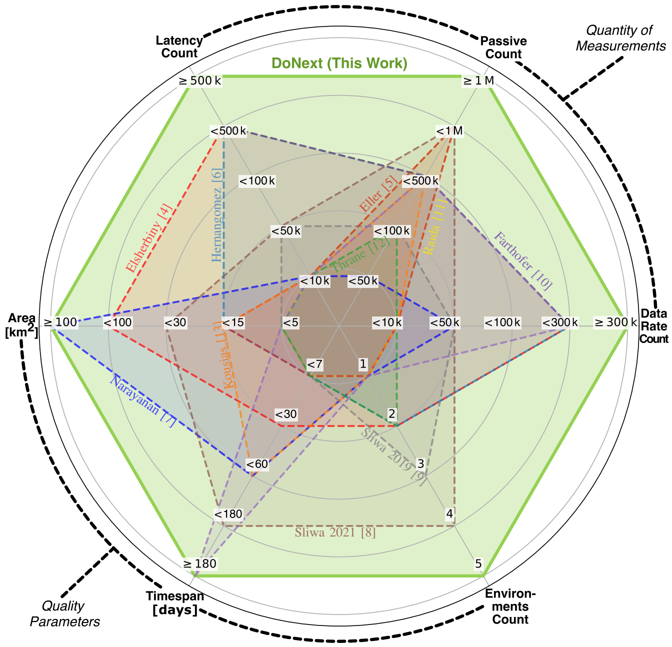

FIGURE 2: Quality and quantity coverage of existing datasets compared to DoNext contributed by this work.

TABLE I: Overview of Related Work Highlighting DoNext's Unique Methodical Aspects

Related Work	Type 4G	5G	Multi MNO	Utilized Device	Protocol TCP	UDP	Direction DL	UL
Narayanan et al. [7]	✗	✓	✓	App	✓	✗	✓	✗
Elsherbiny et al. [4]	✓	✗	✗	App	✓	✗	✓	✓
Raida et al. [11]	✓	✗	✗	App	✓	✗	✓	✗
Sliwa et al. [9]	✓	✗	✓	App	✓	✗	✓	✓
Sliwa et al. [8]	✓	✓	✗	App	✓	✓	✓	✓
Hernangomez et al. [6]	✓	✗	✓	Modem	✓	✗	✓	✓
Eller et al. [5]	✓	✗	✓	Proprietary	✗	✗	✗	✗
Thrane et al. [12, 14]	✓	✗	✓	Proprietary	✗	✗	✗	✗
Kousias et al. [13]	✓	✓	✓	Proprietary	✓	✗	✓	✓
Farthofer et al. [10]	✓	✗	✗	Modem	✓	✗	✓	✗
DoNext (This Work)	✓	✓	✓	App & Modem	✓	✓	✓	✓

DL: Downlink UL: Uplink

data rate, User Datagram Protocol (UDP) streams may not represent typical application behavior. Regardless of the selected configuration, data rates in mobile networks are subject to fluctuations due to complex interrelations with other users and cells. Thus, many measurements are necessary to depict their statistical characteristics accurately.

This may be even more critical for latency measurements, as they do not benefit from temporal averaging like data rate measurements. Due to their nature, latency measurements only depict the network and channel state at a single point in time. As this might change, the continuity of measurements is crucial. While most works performed their studies in a few days [4, 6, 9, 11], only some extended their campaigns over a longer time [8, 10], creating a more robust dataset. In order to understand mobile network mechanics fully, it is vital to perform measurements in an extended area. To evaluate this, we approximated the covered area of the works (cf. Fig. 2). If measurements were conducted only on a single road or round track, the area in between was not counted as covered. As a result, it becomes evident that most works covered only a few areas. Therefore, there is a risk that the collected data cannot be sufficiently generalized. The covered area, timespan and number of different environments can be seen as quality parameters. While a dataset may contain many data points, the significance of these may be reduced due to a lack of quality parameters. Further, it is often unclear exactly how measurements were performed, and replicating campaigns is impossible due to proprietary solutions.

Unlike other datasets, which are often limited to short-term or geographically narrow measurements, DoNext offers long-term data covering urban, suburban, and rural areas with a high measurement density. This distinction is visually evident in Fig. 2, where DoNext achieves the most extensive and most balanced coverage across key dimensions. While some works covered single aspects like a large area or performed campaigns over a long time span, other parameters like the number of measurements are not convincing. By leveraging DoNext, researchers can explore ML-based mobile network predictions in diverse real-world environments while addressing challenges like temporal variability and multi-MNO performance.

B. Mobile Network Measurement Applications

Capable measurement tools and software are crucial for in-depth mobile network studies. As shown in Tab. I, measurement tools can be divided into modem- and smartphone-based hardware. Both are also available in commercial versions with dedicated hardware. However, this work will focus on openly available measurement tools.

Multiple free-to-use applications exist for some kind of mobile network measurements [23, 24]. Different state agencies like [25, 26] also provide applications to test network coverage. While all of these applications feature the ability to measure some parameters, most are restricted in their functionality or adaptability. Users can freely contribute their own data in most apps, but access to aggregated data is often restricted or legally prohibited [23, 24]. At the same time, the capability of performing freely configurable data rate and latency measurements is usually lacking.

The *Android* application *MobileInsight* is able to measure multiple passive signals, and example analyses with *Python* are provided [27]. However, it does not support active measurements. This is also the case for *NetMonster* [28], *SigCap* [29] and *Network Signal Guru* [30].

That is why we have developed our own measurement application, *TU Connectivity Monitor (ConMon)* [31, 32]. As *NetMonster* is based on the open-source *NetMonster-Core* library [33], we included it in our application to verify queried passive KPIs via the *Android* Application Programming Interface (API). *ConMon* uses a service and multi-threading to issue measurements regularly. Additionally, change listeners for relevant mobile network parameters are used. Unlike other applications, *ConMon* can be configured to capture passive network parameters at the current location and measure the data rate using *iperf3* and the Round-Trip-Time (RTT) via Internet Control Message Protocol (ICMP). Queried data is combined and exported to multiple CSV files, organized in sessions. These can be compressed and uploaded via a Representational State Transfer (REST) API. This format ensures human-readable data and easy usability with most tools. A session can be started manually or using so-called geofences, which automatically stop acquisition in predefined areas. An updated version of *ConMon* is proposed in this work and is freely available to download and use [2]. This way, we want to enable others to generate their own measurement data or extend DoNext.

III. Selected Mobile Network Machine Learning Methods

Mobile networking spans a wide area of research, from physical layer signals to application layer investigations. ML is vital for extracting those insights across domains. The main focus of ML in this work is predictive Quality of Service (pQoS) and radio propagation modeling. For these tasks, different methodologies are discussed.

A. Machine Learning for Mobile Network Key Performance Indicator Prediction

Predictive QoS is a well-developed research area. Especially different approaches for data rate predictions have been evaluated. Tree-based prediction models, such as Random Forests (RFs), are commonly used, as demonstrated in [34–37]. Also, time-series prediction has been evaluated in conjunction with RFs [38]. An RF model is trained by constructing multiple decision trees and averaging their results in a second step. This ensemble learning approach decreases the effect of single decision trees tending to overfit. Some works also used boosting-based methods such as Gradient Decision Boosted Tree (GDBT) [34, 39] or Xtreme Gradient Boosting (XGB) [40]. Boosting increases the impact of weak learners, which might better predict rare occasions that strong learners do not cover. Artificial Neural Networks (ANNs) are common models for learning on massive datasets and are also utilized for data rate predictions in mobile networks [8, 9, 40]. It contains nodes (neurons) organized in layers, which are interconnected by weighted connections (synapses). Input features are propagated through this network, determining the network's output. During the training process, the weights are altered to fit the needed relation between input features and a label like the data rate. However, all these methods have in common that a feature set is used to predict the available data rate in the immediate future.

Radio Environmental Map (REM)-based prediction approaches overcome this limitation by aggregating a feature set in a given area. REMs consist of a predefined multidimensional grid containing aggregated reference signals or performance metrics based on geographical locations [34]. By utilizing this data, in-advance predictions along known trajectories become possible. The cell width of the REM can be adjusted, allowing a trade-off between resolution and data availability at each grid location.

In addition to data rate predictions, latency predictions have been performed for 4G networks by [41] using Support Vector Machine (SVM), Decision Tree (DT) and Linear Regression (LR) models. It is crucial to predict high latency spikes, as these are not tolerable for some applications. In general, weak learners are better at capturing these rare events. That is why gradient-boosting techniques like Light Gradient-Boosting Machine (LGBM) [15], GDBT or XGB are promising approaches. However, in [15], an ANN-based approach slightly outperformed tree-based methods.

Mostly, less complex models like LR and exponentially weighted or autoregressive integrated moving average are used to benchmark proposed ML models [16, 42]. While some works performed KPI predictions based on some form of simulation [43] or studies in private 5G networks [44, 45], this work will focus on real-world measurements in public mobile networks.

For radio signal strength prediction leveraging geodata, three-dimensional building and elevation data is often transformed into two-dimensional input images representing the propagation environment [5, 46, 47]. Convolutional Neural Networks (CNNs) tend to be used to process these synthetic images appropriately. CNNs are a particular type of ANNs employing convolution operations to effectively process input features (e.g., image arrays) according to the sparse connectivity paradigm. However, it is also possible to extract numerical features from the 2D data and thus enable using tree-based ML methods for predictions, as in [47]. Tree-based models, unlike CNNs, cannot extrapolate, which may limit their effectiveness when applied to new, unseen data. Therefore, we use a CNN-based approach in this work.

Data filtering is crucial for improving the accuracy of ML predictions. For example, while ANNs cannot handle *not-a-number* and extreme values at all, they can also deteriorate the performance of tree-based methods. That is why we limited labels to a maximum of 1 Gbit/s and 100 ms, similar to [15], and set unavailable features to a fixed value before scaling them using a standard scaler. Furthermore, measurements were filtered to include only 5G NSA data.

B. Important Mobile Network Reference Signals

Meaningful filtering is dependent on understanding and interpreting captured signals correctly. Furthermore, understanding the meaning of important reference signals is

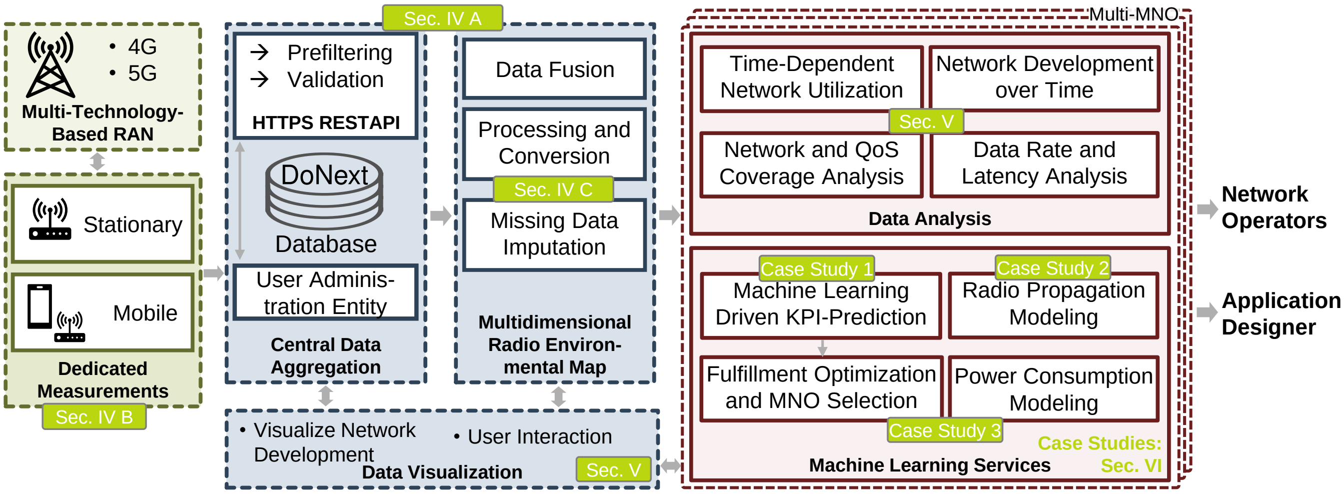

FIGURE 3: Overview of the DoNext system, illustrating the end-to-end data acquisition process, including measurement campaigns, data processing, and analysis for mobile network optimization.

crucial to judging prediction results. For mobile network KPI predictions, signal strength, signal quality, and Signal-to-Interference-Plus-Noise-Ratio (SINR) are essential features. For 4G and 5G networks, the signal strength is mainly represented by the Reference Signal Received Power (RSRP). It is defined as the linear average over a specific set of reference signal resource elements transmitted by the Base Station (BS) [48]. In contrast to the RSRP, the Received Signal Strength Indicator (RSSI) measures the signal power over N resource blocks [48]. Hence, it is the sum of the powers of all signals S_{total} sent by the BS, interference I_{total} from other users and neighboring BSs, and background noise N_{total} present, as shown in Eqn. (1):

$$\text{RSSI} = S_{\text{total}} + I_{\text{total}} + N_{\text{total}} \tag{1}$$

As noise and interference complicate transmissions, an important measure is the SINR, defined as in Eqn. (2):

$$\text{SINR} = S/(I + N) \tag{2}$$

However, there is not just noise and interference influencing mobile network communication. Competition for the available resource blocks and the overall signal quality are also relevant factors. The Reference Signal Received Quality (RSRQ) represents the signal quality, defined as in Eqn. (3):

$$\text{RSRQ} = \frac{N \cdot \text{RSRP}}{\text{RSSI}} = \frac{\text{RSRP}}{\text{RSSI}/N} \tag{3}$$

It sets the measured signal strength in relation to the theoretical power measured if all resource blocks would be occupied. If no noise and interference are present, the RSRQ would be −3 dB for LTE and 0 dB for New Radio (NR), provided the cell is not utilized in the downlink [49]. Thus, the RSRQ can be viewed as an indicator of cell utilization. As the RSSI measures the received power over a wide bandwidth, interference and noise influence the measurement, especially in low signal strength situations, so the RSRQ is not a direct measure of the downlink cell utilization.

IV. Proposed Mobile Network Digital Twin Approach

As underlying ML methods rely on accurate data, digital twins depend highly on up-to-date mobile network measurements. To create a digital twin capable of supporting future mobile applications, we developed a system architecture that integrates automated data acquisition, processing, and analysis.

A. The Automated Cellular Measurement System

We developed a cellular measurement system that automatically performs and processes measurements [32]. The system architecture consists of three main components: data acquisition, data processing and validation, and advanced analysis. With the help of dedicated measurement campaigns consisting of mobile and static devices as well as a crowdsensing-enabled measurement application (cf. Sec. VI B), up-to-date data is captured and uploaded to a central server entity. Uploading data is restricted to previously authorized users, ensuring integrity. Before inserting the data into a relational database, prefiltering and validation of uploaded data is performed, as shown in Fig. 3. This step ensures that no invalid data like, e. g., too low signal strength measurements or data with an insufficient location accuracy, is uploaded.

The aggregated data is used to generate multidimensional REMs, providing a spatial representation of network performance metrics. In this step, imputation of missing data and data fusion with external sources can be performed. This way, the measured data can be verified. Based on mobile network use cases, mappings to QoS requirements are generated.

The resulting KPIs can then be predicted with ML methods (cf. Sec. VI). Furthermore, power consumption can be modeled based on an application's communication behavior and location. The recorded data can also be used to train and refine ML models dependent on large datasets for appropriate training. *DRaGon* [46], an ML-based mobile network signal strength prediction approach, is evaluated on the data of this work. After training a suitable model, the signal strength in locations without any measurements can be predicted,

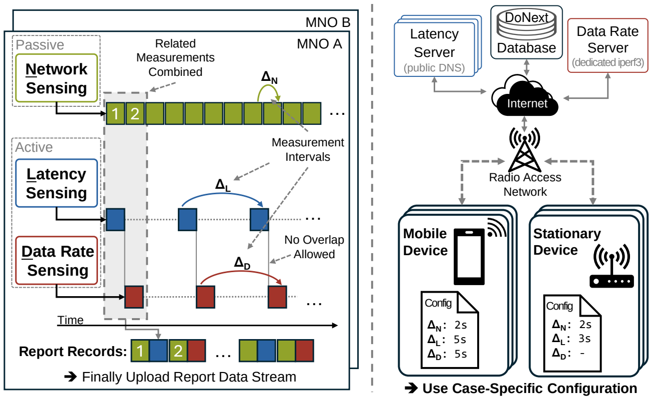

FIGURE 4: Use case-specific scheduling of measurements.

creating a gapless coverage map.

The leveraged knowledge of the mobile network allows to provide crucial information for future mobile network use cases as a service. Due to the gapless coverage map, the feasibility of applications at given locations can be evaluated. This approach also enables MNO selection, optimizing the fulfillment of KPIs. Thus, mobile network-based application planning can be enabled or at least supported, and feedback can be given to network planning by providing connectivity data as a service.

B. Measurement Campaigns and Implementation

We started multiple measurement campaigns with drive tests to optimally cover the Dortmund city area. The measurement procedure covers passive, latency and data rate measurements with individually configurable measurement periods. Matching passive and active measurements are allocated to each other for later analysis. Simultaneous active measurements are excluded, and latency measurements are scheduled to be run directly before data rate measurements. Uploads of results are not performed during other measurements. The software *iperf3* is used to measure the data rate to a dedicated server, while latency measurements are performed to public Domain Name System (DNS) servers via the *ping* command. We collaborated with multiple organizations in the city to perform the measurements:

a) With the help of the local waste deposit company, we were able to equip six garbage collection vehicles with our *Android* measurement application *ConMon*. As the waste of each household has to be picked up regularly, good area coverage is guaranteed with this setup. Every workday, the garbage collection vehicles start at the service yard and complete a predefined route, repeating every two weeks. *ConMon* was configured to automatically start and stop measurements as the vehicles leave the service yard with the help of *geofences*. The default measurement interval shown in Fig. 4 is adopted automatically by the driven velocity. By switching the considered MNOs after some time, all areas were covered with measurements of both networks [50].

b) In order to extend the coverage to areas outside the established garbage track routes, we performed measurements in vehicles of the public order office one year after the measurements with the garbage trucks. These vehicles follow no predefined routes and also drive to remote locations. This way, we aim to validate our previous measurements and unveil changes in the mobile network.

c) Additionally, we deployed dedicated hardware on a suspension railroad track along the university campus [50]. The suspension railroad interconnects several locations on the campus and repeats its course multiple times a day.

d) The dedicated hardware was also used to perform stationary measurements spread in Dortmund for several months to provide data for every time of day.

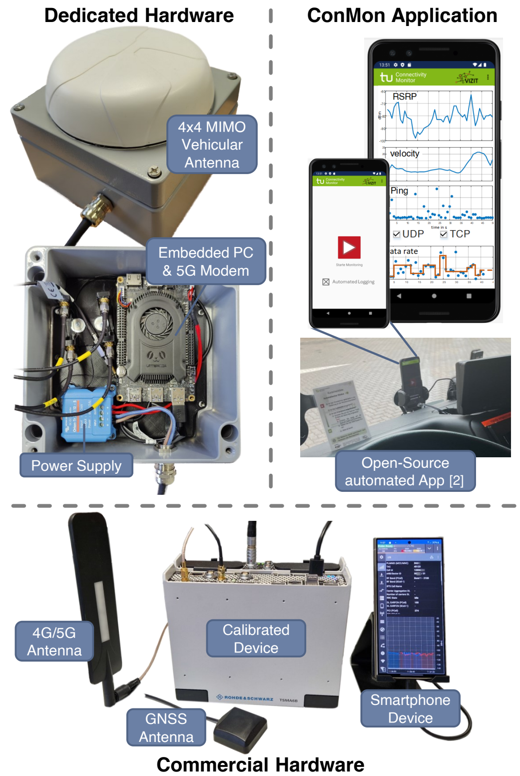

FIGURE 5: Developed systems for automated mobile network measurements used for DoNext measurement campaign (cf. [32, 50]) and commercial devices for validation.

The utilized measurement systems are shown in Fig. 5. Depending on the use case, both have distinct advantages. While the *dedicated hardware* can be deployed in outdoor environments, *ConMon* is easy to use and portable. Due to the smartphone form factor, it can be utilized by most people, thus enabling crowd-sensing approaches. We deployed the app on *Samsung Galaxy S21* and *S22* 5G-capable smartphones. A closer description of *ConMon* is provided in Sec. II B. The dedicated measurement hardware can run without user interaction for a prolonged time and provides more detailed measurements (cf. Tab. II). It is equipped with a capable system on a chip and a *Quectel RM520N* 5G modem connected via a m.2 connector to a PCI interface (avoiding

USB-3 irradiation). Position data is supplied by a Global Navigation Satellite System (GNSS) module supporting multiple constellations and featuring an Inertial Measurement Unit (IMU) for reliable and exact localization. On top of the GNSS module, a power supply is located, as shown in Fig. 5. The described components are enclosed in a watertight enclosure with a 4x4 Multiple Input Multiple Output (MIMO) 4G/5G vehicular antenna on top. For validation, we utilized commercial measurement systems from *Rohde & Schwarz* consisting of a calibrated dedicated device (*TSMA6*) and a smartphone form factor device (*QualiPoc*).

C. Measured Mobile Network Parameters and Key Performance Indicators

During our measurement campaign, we aimed to capture multiple indicators and reference signals of the mobile network. Some of these parameters are semi-static and depend on the network- and cell configuration. Other parameters vary vastly over time. These passive network parameters need to be sampled periodically in order to accurately capture the current state of the mobile network channel. Their availability and maximum temporal resolution depend on the deployed hardware. The measured parameters and their function are explained in Tab. II.

One of the measured parameters is the E-UTRAN Cell Identifier (ECI), specifying the exact sector and Evolved Node B (eNB) for a set operator in a set country [51]. For neighboring cells, the ECI and eNB ID are not reported by the User Equipment (UE), as no connectivity to these cells is established, but they are required to derive the transmitter positions. However, the Physical Cell Index (PCI) of neighboring cells can be measured. In LTE, the PCI is a 9 bit value reused across different cells [52]. Nonetheless, the PCI remains unambiguous in the vicinity of each cell—otherwise, reference signals would overlap, leading to distorted channel estimations. That is why eNB IDs are estimated by comparing the PCI of neighboring cells to existing serving cell measurements in the vicinity. The implementation of the algorithm for this estimation can be found in Appendix A. Incorporating neighboring cell measurements is highly beneficial for analysis and ML. These measurements provide additional data points that capture low signal strength conditions, often overlooked in standard analyses focusing on serving cells alone. Especially in urban environments, low signal strength situations are rare due to a high BS density. Including low signal strength occasions leads to more accurate modeling of bad coverage areas and can improve the robustness and generalization of ML models, especially in cell edge cases (cf. Sec. VI B).

Overall, the proposed measurement approach leverages mobile and static devices for automated measurements, providing data that is processed for later analysis. Measurement campaigns capturing key network parameters ensure comprehensive coverage, enabling the application of ML methods and mobile application planning.

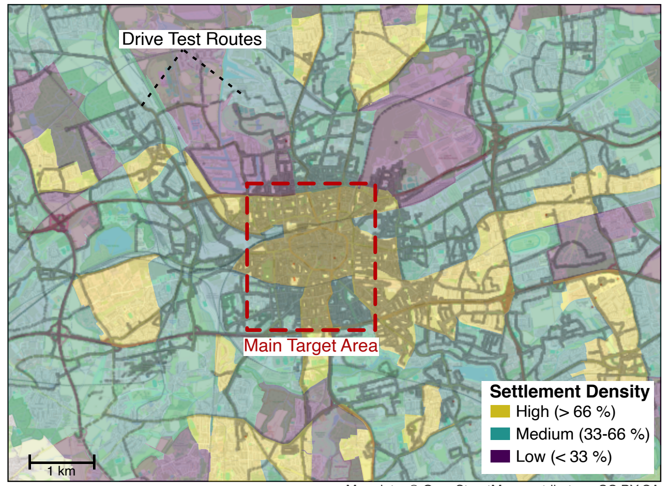

FIGURE 6: DoNext data covering vast parts of the metropolitan area of Dortmund, Germany. Overlaid settlement density data (Share of settlement and traffic area) from [54].

V. Statistical Analysis of the Collected Data

We measured 4G and 5G data in the metropolitan area of Dortmund, Germany, for two MNOs. Dortmund has almost 600,000 inhabitants [53] and is one of Germany's ten biggest cities. Over 22,000 buildings with up to 20 floors are registered in the city's open-data portal in the downtown area [53]. As shown in Fig. 6, we covered vast parts of the city over an area of more than $100\,\text{km}^2$. While the measurement density is higher in the center, which is the main target area, we also covered the main roads in the outer parts of the city. It is illustrated that the measurement area comprises urban, suburban and rural areas by overlaying the settlement density. As described in Sec. III, locations are covered multiple times due to repeated measurement schedules, increasing the measurement density. Over 22,500 km have been driven, resulting in over twelve million passive, six million latency, and 440,000 data rate measurements. The data contains eNBs with 2,600 unique sectors (cell identifiers). In addition to the serving cell parameters, the neighboring cell measurements were recorded, resulting in even more data.

In a comparative measurement study, data points captured by *ConMon* have been compared to commercial mobile network measurement devices (cf. Fig. 5). A lower acquisition frequency of *ConMon* compared to the commercial smartphone device is mitigated by the systematic repetition of measurements. As demonstrated in Fig. 7, comparable measurement accuracy is achieved, underlining the quality of DoNext and the useability of *ConMon* for future campaigns. The antenna used with the calibrated device has an antenna gain of approximately 4 dBi, explaining the higher median RSRP. While the commercial equipment excels in measurement frequency and resolution, our proposed *Android* application is openly useable and scalable for automatic and dispersed measurements.

The collected mobile network data has been converted to

TABLE II: Recorded Parameters of Connectivity Monitor (ConMon) App and Dedicated Hardware.

Parameters	Short Description	Function and Implicit Meaning
Fixed Cell Parametrization (Passive)		
PLMN: MCC & MNC	Mobile country code & mobile network code	Assignment to provider, intrinsic characteristics of the network
ARFCN	Absolute radio frequency channel number	Used carrier frequency, effect on path loss and indirect bandwidth inference
Bandwidth$^{(*)}$	Bandwidth of the current cell	Influences achievable data rate due to available resources
PCI	Physical cell identity [52]	Locally valid identification of (neighboring) cells
ECI	E-UTRAN cell identifier (sector-specific) [51]	Cell-specific characteristics and assignment to base station
TAC	Tracking area code of the cell	Global unique assignment to a cell of an MNO together with cell index
Duplex Mode*	If time or frequency division duplex is used	Duplex by alternating uplink and downlink or by two separate bands
SCS*	Used subcarrier spacing	Tradeoff between resource element size in time and frequency domain.
Time-varying Network Parameters / Reference Signals (Passive)		
Available Technologies	2G, 4G, 5G NSA, 5G SA	The available technologies at the current location
Cell Bandwidths	Sum of the bandwidth of aggregated cells	Higher data rates can be reached by combining multiple cells
RSRP, SS-RSRP	4G/5G part reference signal received power [48]	Path-loss estimation, impact on modulation scheme and data rate
RSRQ, SS-RSRQ	4G/5G reference signal received quality [48]	Utilization and interference from other cells and users
SINR, SS-SINR	4G/5G signal-to-interference-plus-noise ratio [48]	Limits possible modulation scheme and is a measure of interference
Neighboring Cell Data	Signal strength and quality of neighboring cells	Information on possible pending handover and interference
RSSI	Overall received signal strength	Calculation of signal quality together with RSRP
CQI	Reported channel quality for LTE	Sets or indicates downlink modulation type
TA	Propagation distance to base station	Multi-path distance to base station, conclusions about the environment
MCS*	Used modulation and coding scheme	Sets the maximum data rate in combination with the bandwidth
Transmit Power $P_{\text{TX}}{}^{*}$	Measured for multiple uplink channels	Affects UE power consumption and indicates remaining uplink link budget
Rank Indicator*	UE-proposed downlink MIMO	Availability of multiple propagation paths for data transmissions
Active Parameters		
Latency	ICMP round-trip-time to 5 Servers	Response time of the network
Data Rate	Uplink & downlink, TCP & UDP, varying file sizes for TCP (1 MB to 10 MB)	In-depth end-to-end analysis of mobile network capabilities for streaming and file transfer applications.
Other Parameters		
GNSS	Location, velocity, bearing, accuracy	Velocity has an influence on channel characteristics, e.g., Doppler effect
Device name and status	Device name, capabilities and thermal status	Deviation of expected performance
Timestamp	Context information	Influence on measurements due to activity of other users.

*Only available with dedicated hardware

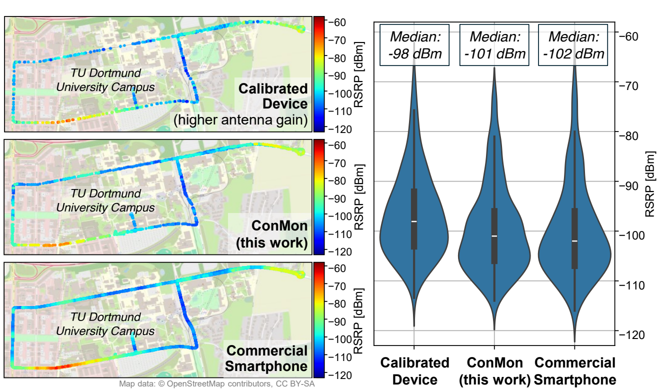

FIGURE 7: Validation of *ConMon* with calibrated commercial measurement devices. Map of the measured RSRP on the left and distribution of measured values on the right.

multi-layer REMs, depicting the location-dependent mobile connectivity (cf. Sec. III). Next to the real-world building layer, exemplary REMs of Dortmund are shown in Fig. 8. They can be divided into passive reference signals and application-level indicators like data rate and latency. Indicators of 4G networks were measured alongside indicators of 5G mobile networks for the two considered MNOs. As can be seen, there are almost no gaps in the data coverage. Most of the remaining gaps are larger private, industrial or rail areas, which cannot or are not allowed to be accessed by vehicles. That is why we focused on the coverage of public roads. Fig. 9a shows the street network coverage by percent as a function of the resolution (maximum allowed distance to the next sample). At a resolution of 50 m, over 95 % of the roads are covered with passive measurements. The density of less frequent active data rate measurements is slightly lower but still only falls below 90 % at high resolutions of under 30 m. Thus, data is available at almost every arbitrary point along the road network in the target area. This high

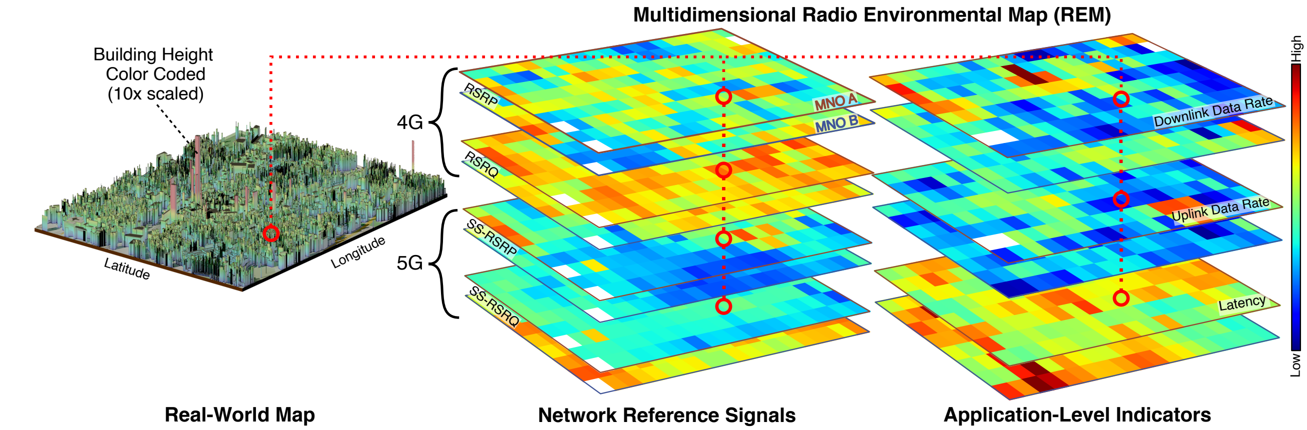

FIGURE 8: Real-world map and multidimensional REM of the main target area (cf. Fig. 6) of DoNext with a cell width of 300 m consisting of various passive and active parameters (Map data: © OpenStreetMap contributors, CC BY-SA).

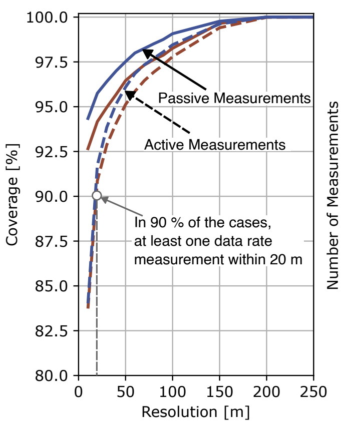

(a) Road Coverage

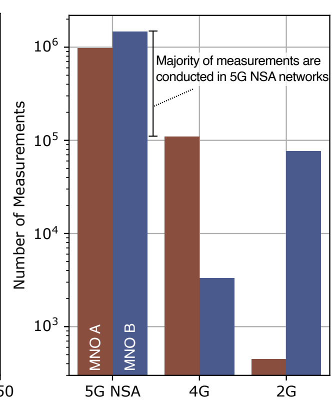

(b) Networks

FIGURE 9: Coverage of the street network in the main target area on the left and number of measurements per network technology and MNO on the right.

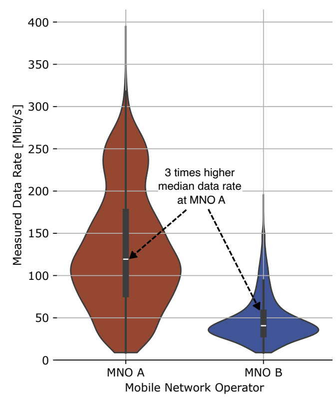

(a) TCP Downlink

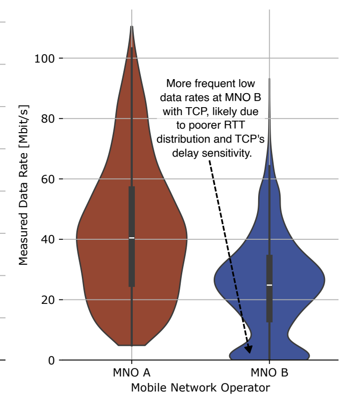

(b) TCP Uplink

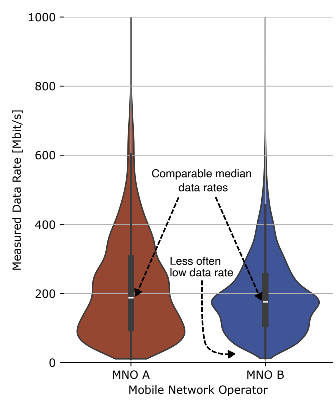

(c) UDP Downlink

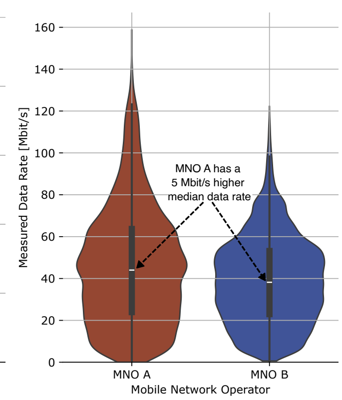

(d) UDP Uplink

FIGURE 10: Distribution of the measured data rate for a payload size of 10 MB in different configurations.

coverage, combined with a long measurement period, enables excellent generalization of findings in the data. All available network technologies in the target area have been covered, as shown in Fig. 9b. However, while most measurements were conducted in 5G NSA networks, depending on the MNO, at some locations, only 4G networks or lower were available.

Data rate measurements were performed with TCP and UDP in the uplink and downlink direction. While TCP is commonly used for reliable data transmission and features a congestion control mechanism, UDP is widely used for data streaming applications without retransmission mechanics. Downlink data rates are measured to be multiple times faster than uplink data rates (see Fig. 10), which can be explained by the typical downlink-driven public mobile networks. This might also be a challenge for future uplink-dependent applications like teleoperation (cf. Sec. VI C) [55]. TCP data transmissions reach a much lower data rate than UDP, especially in the downlink. This behavior is due to the congestion control of TCP, which leads to a slow-start behavior in addition to a throughput limit set by the window-size latency product. For TCP downlink, the data rate at MNO A is 2.7× higher than for MNO B, which is not the case for UDP. As new packets cannot be transmitted with a full transmit window before an acknowledgment is received, the data rate depends on low latency acknowledgments. Thus, the higher data rate for TCP matches the slightly lower latency

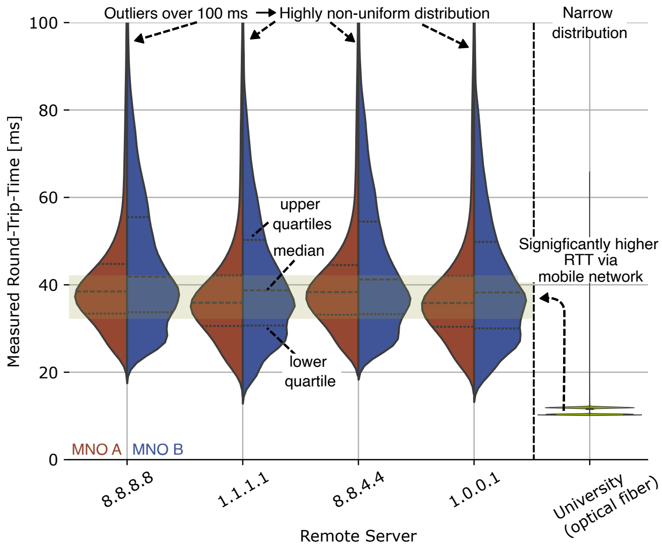

FIGURE 11: Distribution of the average RTT from the mobile network compared to the RTT from a stationary server to different DNS servers.

experienced with MNO A, as seen in Fig. 11. In the case of UDP data rates, MNO A has a 10 Mbit/s higher median uplink data rate, while both MNOs feature the same median data rate in the downlink. Low UDP downlink data rates occur less often for MNO B compared to MNO A.

We measured the average of four ICMP RTTs to four common public DNS servers (cf. Fig. 11). The median latency to all DNS servers is comparable at a set MNO. While the lower quartile latency is similar, the upper quartile of MNO B is higher than that of MNO A for all tested servers, potentially making MNO A better suited for applications reliable on low-latency connections. Different network utilization and configurations could explain the differences between the MNOs. Various network parts, from the radio access layer to the core network, influence overall latency. Compared to the data rate, the latency is a more noisy measure, as there is no averaging over a particular interval. We measured rare outliers well beyond 100 ms, including connection losses, which are not shown in the figure for better readability. These outliers do not occur when measuring the RTT to DNS servers from a static server connected via optical fibers, showing the demanding characteristics of the mobile network.

With the help of our prolonged measurement campaign covering vast parts of the city, network expansion effects and network utilization changes can be uncovered. For this, we analyzed the measured average signal strength in downtown Dortmund from 2019 [9] to 2023 and 2024. While in 2019, still, only 4G networks were available, in 2023 and 2024, 5G NSA was also recorded, as shown in Fig. 12. It can be seen that in the northeast of the area, the signal strength improved over 25 dB from 2019 to 2023, which can be allocated to network expansions. Only minor changes can be seen comparing the LTE RSRP measurements of 2023 and 2024. LTE extension seems to be completed. Comparing the SS-RSRP, network extensions in the south of the selected area become visible. Here, the coverage quality has been drastically increased from a bare availability (RSRP approx. −110 dBm) to a high signal strength connectivity (RSRP approx. −80 dBm), enabling the deployment of higher data rate applications in this area.

Stationary measurements were conducted spread around Dortmund city to get an overview of the daily network activity over time. For this, we selected the TU Dortmund University campus in the south-west, a location near the B1 highway, and local soccer stadium, a location in the inner city at a central square and a location in an inner-city residential area between the city center and the B1 federal road, as shown in Fig. 13. For each location, the RSRQ course over weekdays (blue) and at weekends (red) is displayed, as it is an indicator for the network utilization (cf. Sec. III). It becomes evident that user activity shifts depending on the day of the week. At the weekend, activity tends to be lower and starts later in

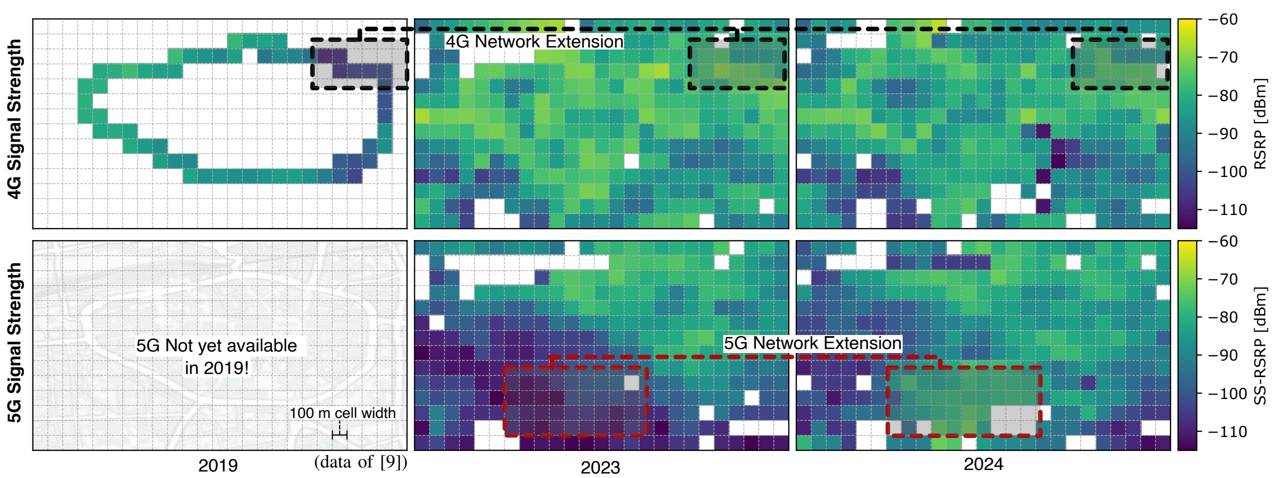

FIGURE 12: Long-term temporal drift of the mobile network signal strength, illustrated by RSRP and Secondary Signal RSRP (SS-RSRP) measurements over time for the 4G and 5G networks of MNO B in Dortmund downtown.

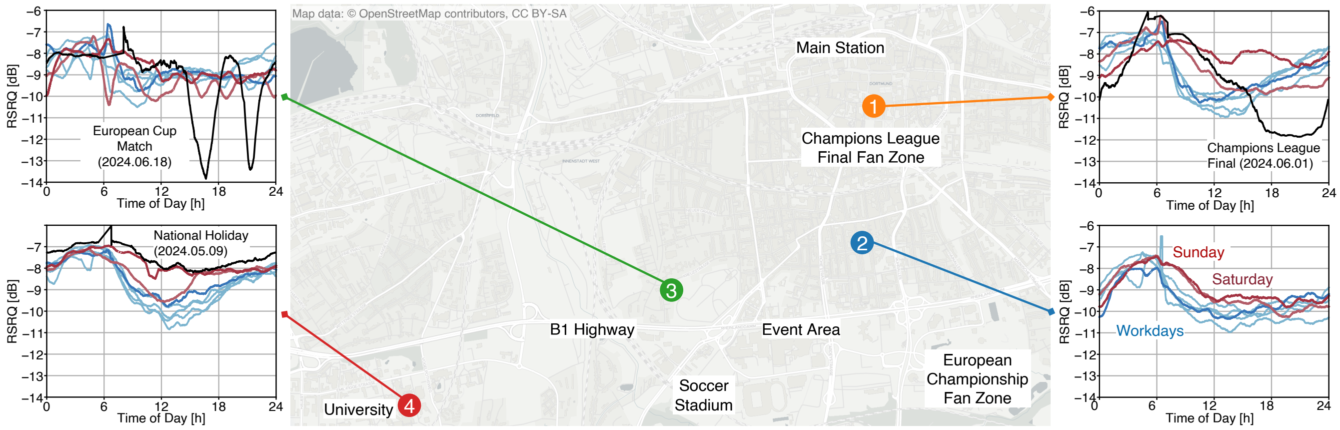

FIGURE 13: Impact of short-term fluctuations in network utilization observed at distributed stationary measurement points. The figure shows daily average serving-cell RSRQ trends for weekdays and at selected special events, highlighting strong deviations caused by atypical network utilization.

the morning. Also, RSRQ courses differ between locations: While at the university, a strong RSRQ dip on weekdays is registered, at location three, an almost constant RSRQ course over the day is recorded.

However, these specific courses differ significantly on special events or holidays, as shown in Fig. 13. For example, during the UEFA Champions League final, public screening events attended by tens of thousands of people took place in and around the city center. As a result, a pronounced dip around the playing time can be seen. A comparable behavior could be recorded before and after UEFA Euro 2024 group stage games in the local stadium. During the playing time, the RSRQ recovered, as the spectators were connected to BSs in and directly around the stadium. While events can result in a higher cell load, the opposite is also possible. During a national holiday, the RSRQ course at the university differs strongly from the usual behavior. With fewer people present at the campus, the overall network load has decreased significantly, resulting in a higher RSRQ. To sum up, the RSRQ roughly follows a periodic course on normal days. However, deviations from the daily course are possible due to events, holidays and possibly further influencing factors.

The authors of [56] analyzed several LTE parameters and concluded the RSRP to have no time-of-day variance in their stationary measurements. In general, we got the same results with our stationary measurements. However, despite being stationary, our RSRP measurements yielded some variation beyond noise effects, as some BSs seem to decrease their transmit power overnight. A reduction of around 3 dB can be measured, as shown in Fig. 14. Especially, cells at location three and the university campus show this behavior. This measure is known to be an energy-saving mechanism for the BS, as the user demand is lower at night. However, the transmit power reduction also affects UEs, as demonstrated in [57] (cf. Sec. VI C). Due to reduced signal strength, UEs might need to change the BS, use a worse Modulation and Coding Scheme (MCS), or even lose the connection if it is

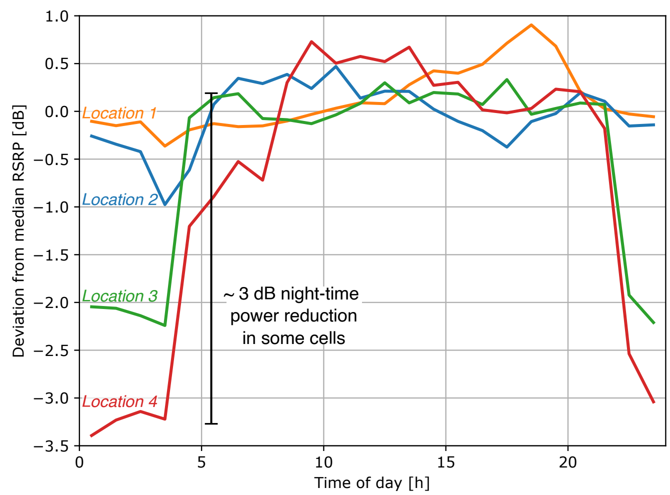

FIGURE 14: Effects of green networking on the received signal strength. Long-term RSRP measurements over the course of the day for MNO A at static locations (cf. Fig. 13).

located at a highly attenuated location.

In sum, our measurements generated a spatiotemporal high-resolution dataset, setting the base for a mobile network digital twin of Dortmund city. The data can be downloaded at [3]. It is divided into processed static, mobile and rail measurements. More detailed information can be found in Appendix B and the dataset description.

VI. Application of Machine Learning on DoNext Dataset

In this section, we will present the usability of the dataset for in-depth ML based on several prediction case studies.

A. Case Study 1: Real-Time Data Rate and Latency Prediction

This case study investigates data rate and latency predictions using ML models applied to the DoNext dataset. By analyzing various models and methods, we demonstrate the feasibility

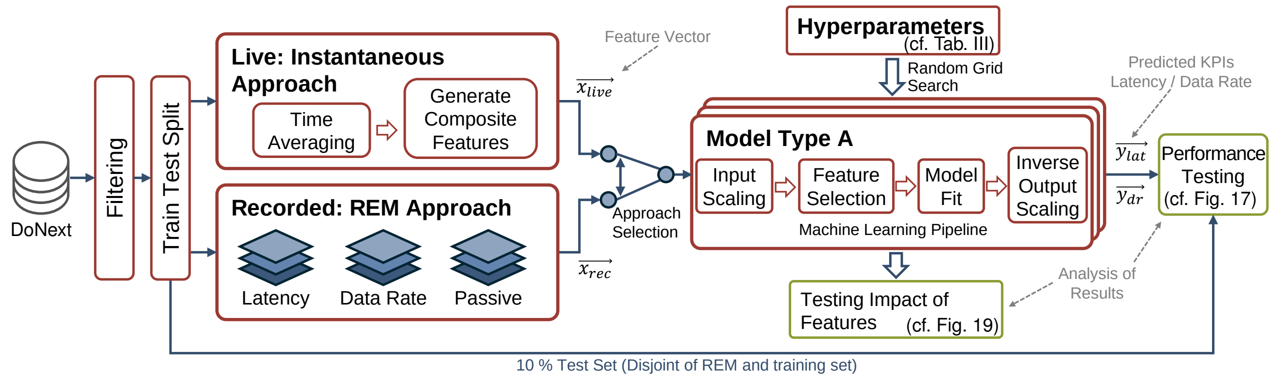

FIGURE 15: Case Study 1: Overview of the machine learning process used for data rate (y_{dr}) and latency (y_{lat}) prediction.

of pQoS in dynamic mobile network environments. Several methodologies for predicting the achievable data rate have been discussed in related works. One is a *live* approach [8] based on currently available passive signals. The advantage of this method is that only signals on the device are utilized, making it rather simple to implement. However, it does not allow for predictions of data rates at future or arbitrary positions. A REM-based prediction can be used for this utilizing *recorded* data. By looking up necessary features for the prediction in a (multidimensional) map, predictions for future trajectories can be made. An important tuning parameter of REM-based approaches is the resolution of the map (cell width), balancing resolution against lookup misses. In this work, we use a fine cell width of 25 m due to the high density of the available data. As the RSRQ is utilization-dependent, we store it in a spatio-temporal map containing time and location-dependent values. In contrast, the RSRP and SS-RSRP are directly mapped to locations, as these are solely location-dependent (excluding nighttime shutdowns shown in Fig. 14). Both methodologies and different ML models are compared in this case study.

For the *recorded* and *live* approach, slightly different features are utilized. For both approaches, the driven velocity, time of day and week of the year are assumed to be known. The *REM* approach includes location, bearing, and time of day. These features are used directly and to select the current REM cell. In the case of the RSRQ, which is a utilization-dependent feature, a spatiotemporal REM is calculated, which also depicts the time of day. The REM-based method can leverage features like maximum and average data rates and latencies from other measurements. In the case of the *live* approach, a rolling average of the RSRP and the RSRQ are calculated from previous measurements in the same measurement session for time intervals of 5 s, 50 s and 500 s. The averaging is aimed at reducing noise effects on these measures. Additionally, the current cell bandwidth, Timing Advance (TA) and ECI are used as features.

The evaluation process of both approaches is shown in Fig. 15. Before feeding the respective feature vector x into the ML pipeline, one approach is selected to predict either the latency y_{lat} or the achieved data rate y_{dr}. Additionally, we used features of both methodologies in a *combined approach*.

TABLE III: Utilized Hyperparameter Grid of the Machine Learning Models for KPI Prediction

Model	Hyperparameter	Hyperparameter Grid
LR	Fit intercept	True, False
ANN	Initial learning rate η	0.6, 0.3, 0.2, 0.1, 0.01
	Momentum α	0.6, 0.3, 0.1, 0.01, 0.001
	Network architecture	[15, 15, 15, 15], [10, 10, 10], [10, 5], [20, 20, 20, 20], [15, 15, 15, 15, 15]
	Number of epochs	1000, 2000
RF	Max depth	10, 39, 158
	Number of trees	50, 325, 600
	Min samples split	2, 4, 8
	Min samples leaf	1, 2, 4
XGB	Max depth	5, 10, 100
	Number of trees	10, 31, 100, 316, 1000
	Min loss reduction γ	0.00, 3.33, 6.66, 10
	Regularization λ	0, 0.25, 0.5, 0.75, 1
All	Number of Features	4, 6, 10, 15, 20
	Grid search Iterations	100

Failed passive measurements with missing values have been replaced with –200 (outside the range of all features) to allow the use of non-tree-based methods. Only 5G NSA measurements are considered. Extreme latency and data rate values, and failed measurements are excluded. In the case of latency prediction, the minimum measured latency to the DNS server '1.1.1.1' is used. UDP measurements with a payload size of 10 MB are used for the data rate predictions.

Irrespective of the proposed methodologies that provide the features, different ML methods for the data rate prediction are evaluated for the prediction step [58]:

- Linear Regression (LR)
- Artificial Neural Network (ANN)
- Random Forest (RF)
- Xtreme Gradient Boosting (XGB)

They are selected to cover the most common models used in this area of research (cf. Sec. III A). The available measurement data is split into train, test and validation sets. Ten percent of all measurements are used for testing. Of the remaining data, 10 % of the samples are used for validation, and the other samples are used for training and REM generation. In order to compare instantaneous and REM-based predictions, samples used for REM generation are also excluded from the instantaneous prediction.

A random grid search is performed for each model, optimizing the Root Mean Squared Error (RMSE) on the validation set. The utilized grid is shown in Tab. III. Linear models generate relatively simple multidimensional linear functions to fit the output. Thus, they have a limited number of hyperparameters, like whether the intercept is fitted, enabling it to predict non-centered data. More complex models like ANNs have a higher number of hyperparameters. While the network architecture defines the overall structure of the ANN layers, the initial learning rate η and momentum α alter the learning process. Finally, a maximum number of epochs stops the training process after a defined number of iterations. Tree-based models like RF and XGB are altered by the number of trees and the maximum depth allowed for these trees. In the case of XGB, a regularization term λ and a minimum loss reduction γ are added to reduce possible overfitting during model training. For the RF model, overfitting is handled by a minimum number of samples needed for a split or a leaf. All ML evaluations are performed with *scikit-learn* [58]. In order to allow automatic feature selection as part of the hyperparameter tuning step for all models, a custom random feature selection based on permutation importance is applied after input scaling, as shown in Fig. 15. The features with the lowest importance are removed until the targeted (randomly selected) number of features is reached (cf. Tab. III). After fitting the model, an inverse output scaling is applied.

In Fig. 16, measured values are scattered above the KPIs predicted with an XGB model for both MNOs. The green line represents a perfect prediction without under- or overprediction. As can be seen, there is no tendency for under- or overpredictions for data rate and latency. However, a 90 % quantile area is marked, showing uncertainty present in the prediction, which increases with larger values.

Different ML models yield partly comparable results. While the LR model performs the worst, tree ensemble methods outperform the ANN model for data rate and latency predictions, as shown in Fig. 17. The difference between the tree-based methods DT, RF and XGB is minimal. While the *recorded* approach manages to predict the data rate and latency without access to current measurements and thus can be used for in-advance predictions, it performs slightly worse than the *live approach*. That is why the latter should be preferred if live data is available. By combining both approaches, only a diminishing improvement in prediction performance is reached, which is why combining approaches is not further considered. In general, the RMSE is about 10 % of the respective maximum value, similar to the results in [8]. In the downlink, a more than 20 % lower RMSE is reached at MNO B compared to MNO A. This behavior can be explained by the achieved data rate, which is, on average, lower for MNO B (cf. Fig. 10c). The opposite behavior can be seen in latency predictions, where lower latencies are measured for MNO A.

While the RMSE of latency predictions is significantly lower than for data rate measurements, their relevant value range is also lower. As a consequence, latency predictions can be seen as, in general, more difficult than data rate predictions.

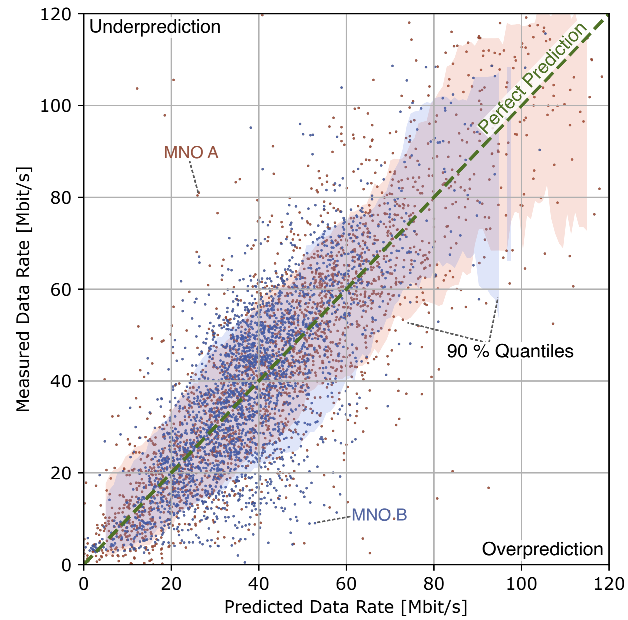

(a) Uplink Data Rate (UDP)

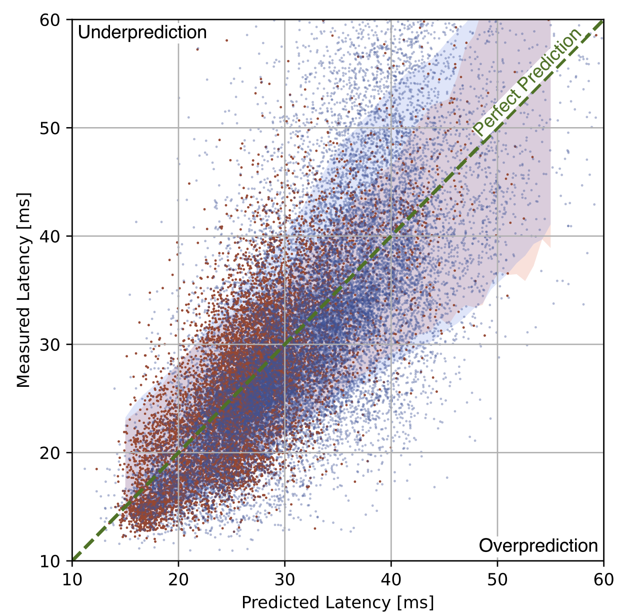

(b) Round-Trip-Time ('1.1.1.1')

FIGURE 16: Scatter plot of actual over predicted data rate and minimum latency with 90 % quantile areas for both MNOs using the XGB model. (Case Study 1)

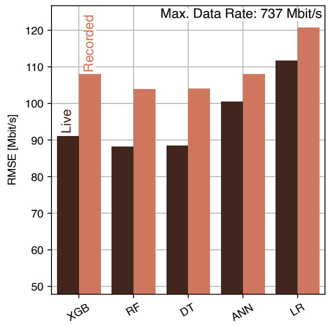

(a) MNO A downlink

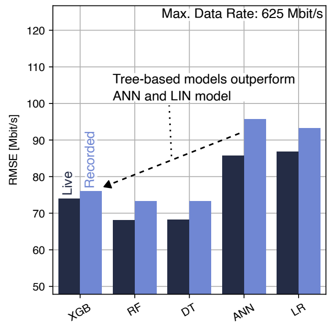

(b) MNO B downlink

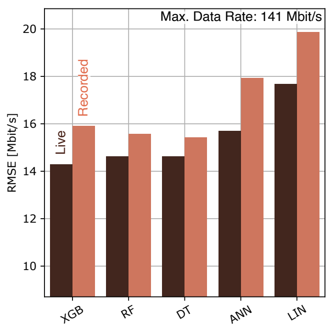

(c) MNO A uplink

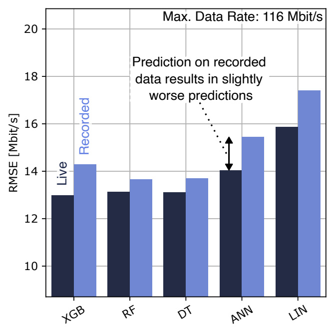

(d) MNO B uplink

FIGURE 17: UDP data rate prediction performance using different methods and data sources. Note: The scale of the downlink and uplink subfigures differs. (Case Study 1)

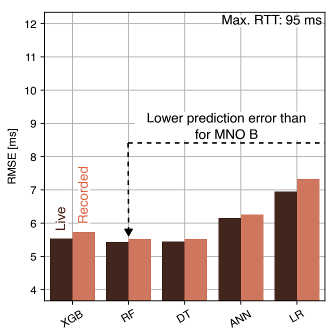

(a) ICMP RTT MNO A

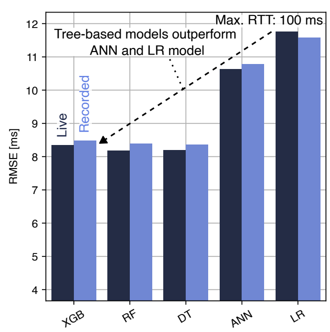

(b) ICMP RTT MNO B

FIGURE 18: Performance of latency prediction using different methods and data sources. (Case Study 1)

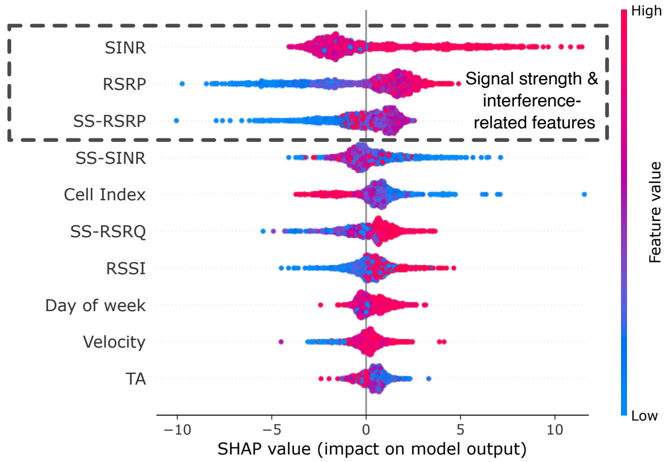

(a) Data Rate Prediction

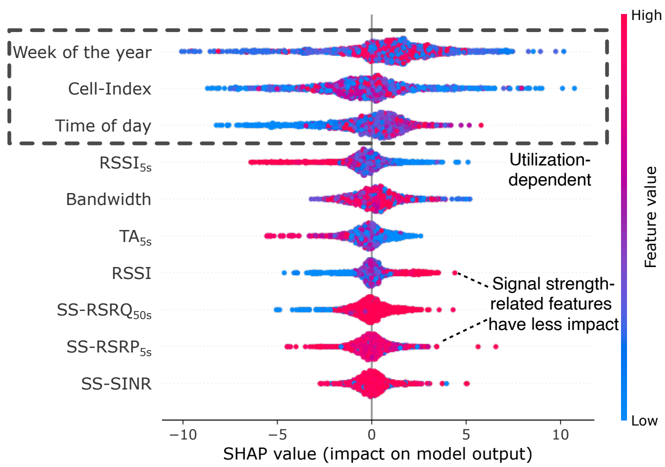

(b) Latency Prediction

FIGURE 19: SHapley Additive exPlanations (SHAP) for *live* approach features of downlink data rate and latency predictions for MNO B, showing the direction, in which the features influence the model output. (Case Study 1)

As the latency is not measured over a set time interval like the data rate, short-time effects might have a higher impact on the latency and introduce noise. Consequently, the output should be less dependent on the signal strength or modulation scheme. Latency measurements are rather more dependent on network utilization and internal routing. In the latency distribution shown in Fig. 11, it can be seen that the median RTT is just below 40 ms. However, there are outliers exceeding 100 ms. Thus, predicting the RTT is an unbalanced prediction task.

In order to understand our ML results, we show the SHAP feature importance and impact on the model output for the ten most important features for data rate and latency predictions in Fig. 19. SHAP provides the additive impact of features (SHAP score) on the model output for each prediction sample and is derived based on game theory [59]. The features are ordered by their mean absolute SHAP score from top to bottom. As in [15], we found high importance of the *week-of-the-year* feature in our predictions, which could indicate a similarity of the latency measurements conducted. Regarding data rate predictions, we yield comparable results to previous works [8, 32], indicating reproducibility between datasets: Signal strength-related features like the SINR and (SS-)RSRP yield the highest impact on the model output.

To sum up, ML can be used on DoNext data to predict the achievable data rate and latency with the help of REMs or by using current passive mobile network measurements. This knowledge can be used to optimize transmission occasions (pQoS) or improve safety by performing communication-aware routing and enhanced application planning.

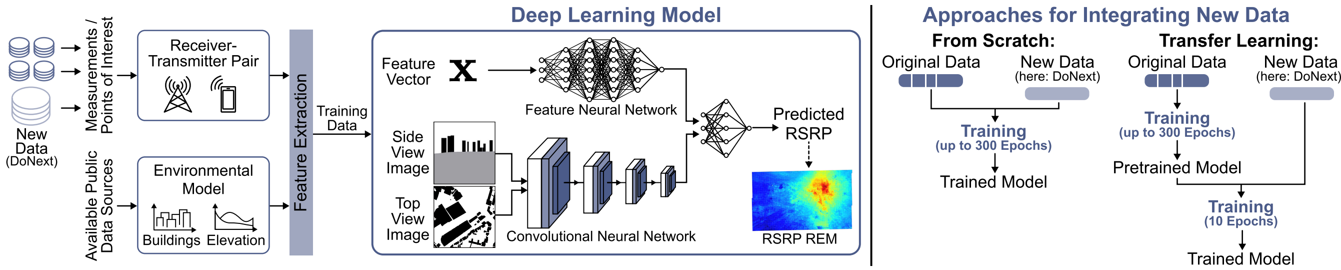

FIGURE 20: Case Study 2: Simplified architecture of the DRaGon model with schematic visualization of training approaches when including new data for derivation of radio environmental maps.

B. Case Study 2: Geodata-based Radio Propagation Prediction with Transfer Learning

Besides high-level KPI prediction, the DoNext data can also be used to train ML-driven signal strength predictions like DRaGon [46]. This means the data can be used to predict the signal strength at locations with unknown connectivity. Additionally, the derived DRaGon model can be used to impute gaps at locations without measurements, like in restricted areas, thus improving network planning. An overview of DRaGon's architecture can be seen in Fig. 20. The DRaGon approach aims to predict the RSRP given a receiver-transmitter pair. A 3D model of the scenario is built based on publicly available geoinformation to incorporate environmental information. This includes building and elevation data. In the feature extraction process, two synthetic black-and-white images are generated: One showing the side view of the direct path and one showing the top view of the receiver. In addition, a feature vector $\mathbf{x}$ is derived containing 13 features from different domains, including channel-specific, relative position, and direct path features. The deep learning model consists of a CNN with six convolutional layers that process the image inputs, an ANN with four hidden layers that process the feature vector $\mathbf{x}$ in parallel, and an ANN with one hidden layer that outputs ΔL by processing the latter outputs. ΔL serves as a correction of the 3GPP Urban Macro (UMa) B Non-Line-of-Sight (NLOS) channel model [48].

Representative data is required to train the model. Previously, the RSRP of serving cells was used to train the prediction model, omitting low signal strength situations. To further improve the accuracy of DRaGon, especially in low signal strength areas, this work uses neighboring cell data in addition to serving cell data. As described in Sec. IV C, the eNB IDs of neighboring cells are estimated using Alg. 1.

In the following, the performance of the DRaGon method on the DoNext dataset is investigated. Therefore, two different training approaches are considered (cf. Fig. 20). When adding new data to the process, this can be done by retraining DRaGon's deep learning model from scratch, meaning that the original data from [46] and the new DoNext data are concatenated. Alternatively, training can be performed in a transfer learning fashion, where the model trained on the original data is continued to be trained on the new data for a few epochs.

For both approaches, we tested different data aggregations (see Fig. 21) by evaluating a hold-out set consisting of 10 % of the gridded DoNext data. The simplest approach is to use the pre-trained DRaGon model, as no training is required. However, its predictions on the new unseen data lead to a relatively high RMSE of 14.6 dB. Since the predictions of the empirical benchmark model, namely 3GPP UMa B NLOS [48], have an even poorer RMSE of 23.2 dB, the prediction task appears to be significantly more challenging. It requires the inclusion of DoNext data in the training process of the model. Due to the huge size of the DoNext dataset (375,000 samples for training), we also consider an approach where only 10 % of these samples are utilized. For the latter, an RMSE of 9.1 dB is achieved on the test data, while the RMSE

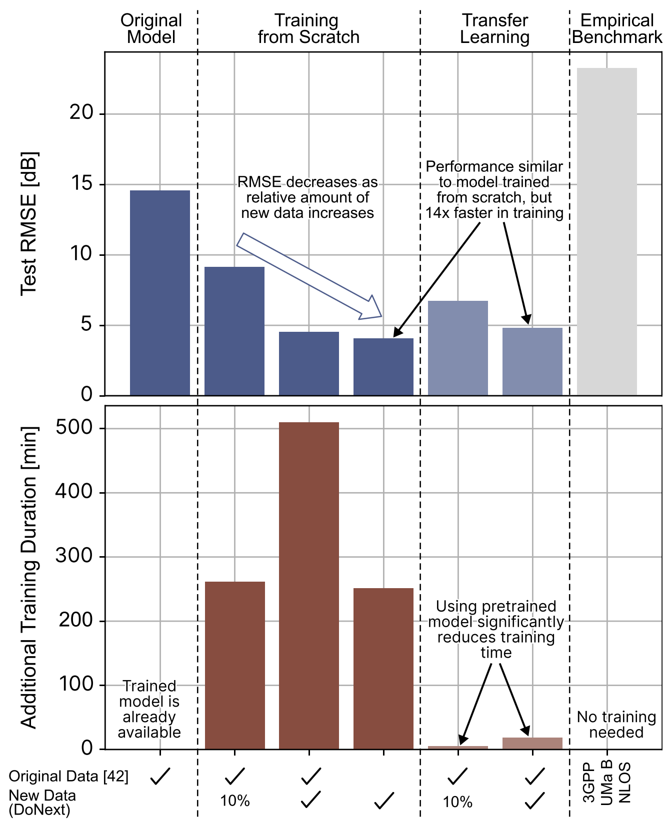

FIGURE 21: Comparison of different DRaGon versions when tested on a DoNext hold-out set regarding their test RMSEs and training durations. (Case Study 2)

can be reduced to 4.5 dB by including all available DoNext samples in the training process, but at the cost of twice as much training time. We also trained the model solely on the DoNext data, yielding the best test RMSE of 4.1 dB. Although the recorded training times are manageable, considering that the model has to be retrained regularly as new data becomes available, the training takes rather long. In the case of transfer learning, the model is continued to be trained on the DoNext data for ten epochs with a learning rate of 10^{-4}. While the model trained on only 10 % of the data is significantly better than its trained-from-scratch equivalent with an RMSE of 6.7 dB, the model trained on all data is slightly worse than its training-from-scratch equivalent with an RMSE of 4.8 dB. However, the training time is significantly shorter and is reduced to only 4.4 and 17.5 min, respectively. Overall, it can be said that even the inclusion of smaller datasets in training can significantly improve DRaGon's prediction accuracy on unseen data. Furthermore, transfer learning has proven to be a valid option, particularly when there is limited time to retrain the model.

As already mentioned, DRaGon can be used to predict the signal strength at locations with unknown connectivity to generate comprehensive REMs. An example can be seen in Fig. 22. As a reference, the REM on the left depicts the measured data for one eNB. On the right, the REM for this particular BS based on the DRaGon predictions when trained on the original, and the DoNext data is shown. Such maps can assist network operators in identifying low signal strength areas and optimizing BS placement to improve overall network coverage. Due to the sparseness of the measurement REM, the predictions and measurements can only be compared at specific locations. Overall, the DRaGon model demonstrates a generally high degree of accuracy in replicating the measurements, with a few exceptions. One such example is the broad street canyon running south from the eNB, where DRaGon tends to underestimate the RSRPs. In order to obviate such effects, a model carrying out actual imputation of the existing measured values and integrating known neighboring values seamlessly into the prediction process could be developed in the future.

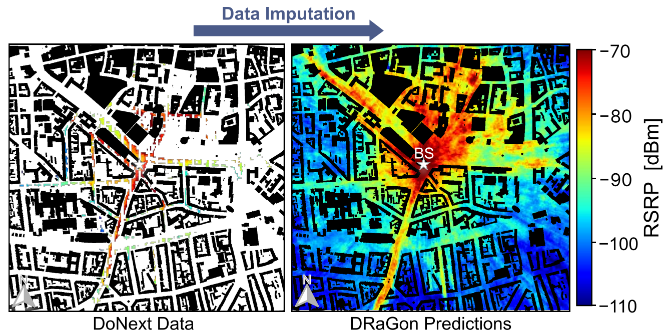

FIGURE 22: DRaGon-based signal strength prediction generating area-wide connectivity maps. (Case Study 2)

C. Case Study 3: Multi-MNO Networking and Target Area Selection

As future smart city applications have demanding requirements, deployments around the city might not be feasible with a single MNO at all locations. Context-aware transmissions based on pQoS are often impractical due to marginal delay tolerance, and there may be a need to deploy certain applications nonetheless. Additionally, battery life remains a major concern for stationary deployments and mobile users. This case study analyzes the potential benefits of switching between multiple MNOs to improve the fulfillment of application requirements and reduce power consumption.

Varying BS locations of different MNOs lead to different signal strength distributions, as can be seen in Fig. 24. In this figure, REMs (100 m cell width) of different KPIs, such as the SS-RSRP (on the left), are shown for MNO A and B in the Dortmund city area. Below the individually measured metrics for each MNO, the improvement by utilizing multi-MNO networking is shown. At some locations, a difference in signal strength of up to 40 dB can be observed. While one network may be underdeveloped or overloaded at some locations or periods, networks of other MNOs may be capable of carrying further load. The difference in the signal strength in some areas is reflected in reduced data rates, as e.g., can be seen at the annotated location in Fig. 24. While the uplink is especially sensitive to higher path loss, the downlink data rate also depends on other factors (cf. Fig. 19a).

As a higher path loss necessitates an increased transmit power, UE power consumption rises drastically at locations with low signal strength, as demonstrated in [60]. A comparison of the power consumption with both MNOs can be made by assuming a set uplink application. Here, a continuous data rate of 10 Mbit/s deployed on a *Quectel RM520N* modem in the n78 band modeled as in [60] is assumed. This setup represents a typical high-quality video streaming application.

At locations with a simultaneously low uplink data rate and signal strength, the power consumption is exceptionally high, as shown in Fig. 23. Switching the MNO can avoid these situations and reduce power consumption. Switching the MNO is especially effective at extreme power consumption locations. In the average case, an improvement of around 15 % can be achieved, as depicted in Fig. 24. Also, achievable uplink data rates can be improved. While the average improvement is restricted due to good coverage in the target area, significant improvements of about 40 % are possible at low data rates. This is especially important if minimum application requirements are at risk of not being met and can be overcome by multi-MNO networking.

To conclude, multi-MNO networking can improve the data rate and simultaneously reduce overall power consumption by preventing high transmit power occasions. This can help enable demanding applications like high-quality video streaming and teleoperation in larger areas. By communication-based route planning and MNO selection, the most optimal, secure trajectory for teleoperation can be estimated.

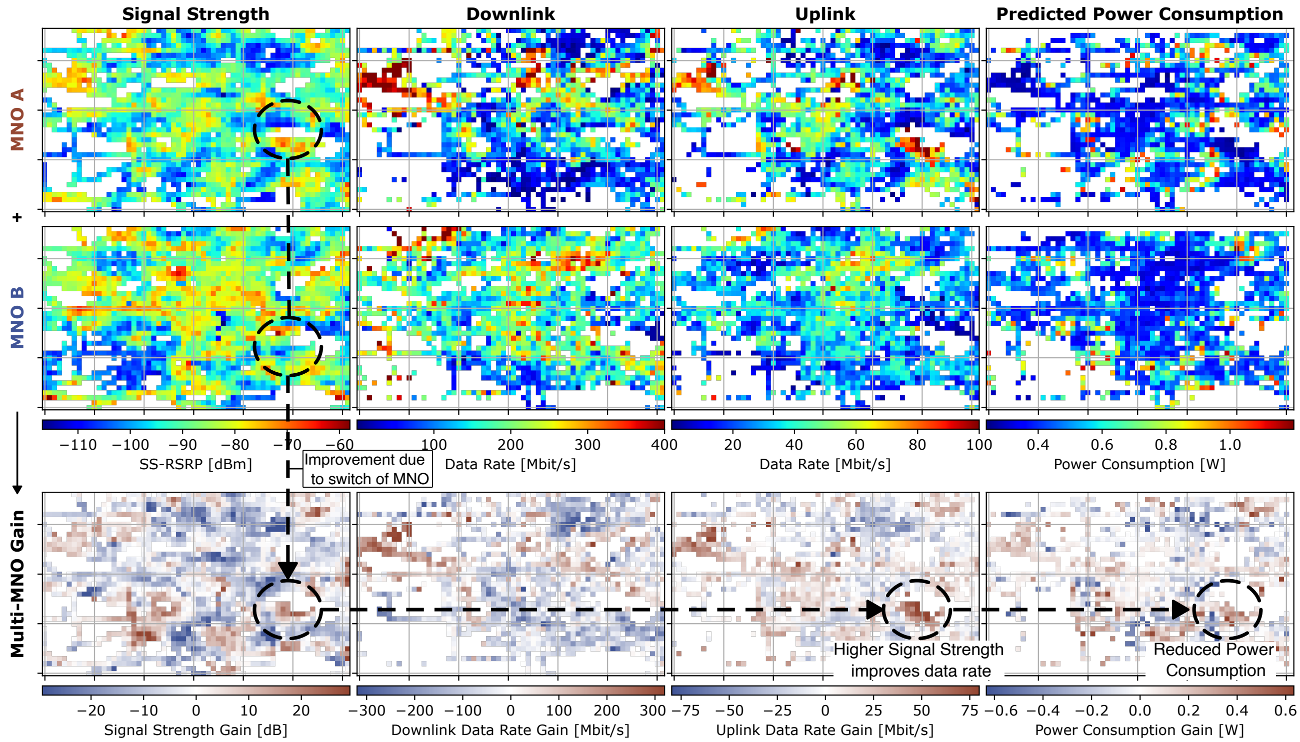

FIGURE 23: Case Study 3: Multi-MNO networking gains for different KPIs in the target area. Measured multi-MNO signal strength, data rate and predicted power consumption for an example application displayed on top.

VII. Conclusion

In this work, we introduced a comprehensive measurement dataset combined with the tooling needed for collecting mobile network quality data. Together, the overall system forms a mobile network digital twin of Dortmund, Germany.

Our dataset, DoNext, offers an unprecedented number of active and passive measurements of mobile and static devices. It allows for in-depth data analysis, change monitoring and the application of advanced ML models. We demonstrated that KPI and signal strength prediction models can be trained and evaluated using this dataset, resulting in more generalizable models. The dataset helps enable future mobile network applications like teleoperation by providing detailed connectivity information. Additionally, it serves as a valuable resource for other researchers to conduct data-driven studies on new ML algorithms. The proposed scalable measurement system is adaptable and can be applied to other locations for further studies. DoNext [3] and the developed measurement application *ConMon* [2] are made openly available.

In the future, we will extend our dataset by additional measurement campaigns and coverage of more areas. That will further validate and enhance the robustness and generalizability of our ML models.

VIII. Appendix

A. Estimating eNB Assignment Based on PCI Data

By iterating over all neighboring measurements C_{neigh} of a specific MNO and matching close serving cell measurements C_{serv}, the corresponding eNB ID of the neighboring cell can be assigned (cf. Alg. 1). In order to filter out incorrect assignments, the cell data (e.g., frequency) is matched, if available. Furthermore, the matching measurements $C_{\textbf{match}}$ are filtered by a maximum distance d_{max} (here 8 km) from the closest serving cell measurement to the neighboring measurement n. If multiple candidate eNBs remain, it is tested whether the proportion of measurements of one eNB is bigger than a majority threshold M_T (here 95 %). In this case, that eNB ID is selected for n. Otherwise, the eNB ID of the closest point in C_{match} is selected. This approach reduces the impact of potential outliers in the measurements.

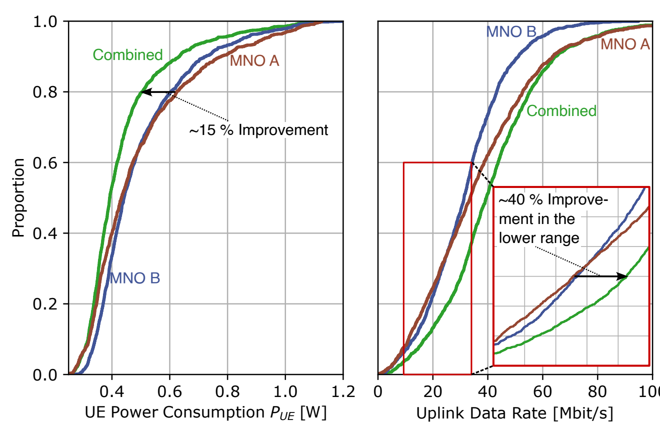

FIGURE 24: Empirical Cumulative Distribution Function (ECDF) of the multi-MNO improvement of power consumption and data rate from Fig. 23. (Case Study 3)

Algorithm 1 Estimation of Neighborcell NB ID

Input: C_{neigh}, C_{serv}, d_{max}, M_T

for all $n \in C_{\text{neigh}}$ **do**
  $C_{\text{match}} \leftarrow$ matchByPCI(C_{serv}, n.pci)
  $C_{\text{match}} \leftarrow$ filterByChannelData(C_{match})
  $C_{\text{match}} \leftarrow$ filterByDistance(C_{match}, d_{max})
  $\text{NB}_{\text{Count}} \leftarrow$ countNBOccurances(C_{match})
  if NBIDExceedsThreshold(NB_{Count}, M_T) **then**
    n.NBID $\leftarrow$ getMajorityNBID(C_{match}, NB_{Count})
  else
    n.NBID $\leftarrow$ getClosestNBID(C_{match}, n)
  end if
end for

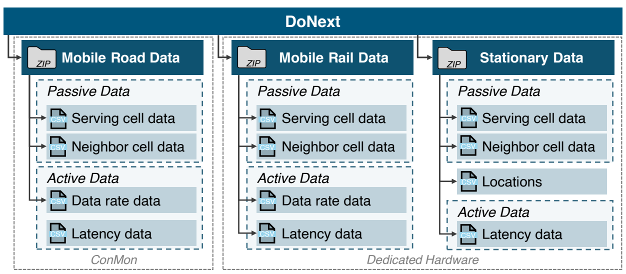

FIGURE 25: DoNext dataset file structure.

B. Structure of DoNext Data

The openly accessible DoNext dataset [3] is divided into three categories: mobile, static and rail measurements, each separately available for download. As shown in Fig. 25, the data is further structured into individual CSV files. Each file begins with column headers in the first row, followed by the actual data, separated by semicolons.

Each measurement file includes position data in additional columns, except stationary measurements. In the case of stationary data, the positions are encoded in a separate file. Passive data, which does not require data transmissions, is available in dedicated files. The most recently measured passive data is added to the active data files as separate columns. This integration is intended to improve usability and reduce familiarization time. Exact dates and times have been removed from the mobile measurements for privacy reasons. An explanation of all columns of the files can be found in [3], while specific signals are summarized in Tab. II.

REFERENCES

[1] J. Johansson, W. A. Hapsari, S. Kelley, and G. Bodog, “Minimization of drive tests in 3GPP release 11,” *IEEE Communications Magazine*, vol. 50, no. 11, pp. 36–43, Nov. 2012, doi: 10.1109/MCOM.2012.6353680.

[2] H. Schippers, S. Böcker, C. Wietfeld, “TU Connectivity Monitor (ConMon),” https://github.com/tudo-cni/conmon, 2024.

[3] ——, “DoNext open-access mobile network dataset,” https://https://tiny.cc/DoNext, 2024.

[4] H. Elsherbiny, A. M. Nagib, H. Abou-zeid, H. M. Abbas, H. S. Hassanein, A. Noureldin, A. Bin Sediq, and G. Boudreau, “4G lte network data collection and analysis along public transportation routes,” in *Proc. IEEE Global Communications Conference*. Taipei, Taiwan: IEEE, Dec. 2020, doi: 10.1109/GLOBECOM42002.2020.9348031.

[5] L. Eller, P. Svoboda, and M. Rupp, “A deep learning network planner: Propagation modeling using real-world measurements and a 3D city model,” *IEEE Access*, vol. 10, pp. 122 182–122 196, Nov. 2022, doi: 10.1109/ACCESS.2022.3223097.

[6] R. Hernangómez, P. Geuer, A. Palaios, D. Schäufele, C. Watermann, K. Taleb-Bouhemadi, M. Parvini, A. Krause, S. Partani, C. Vielhaus, M. Kasparick, D. F. Külzer, F. Burmeister, F. H. P. Fitzek, H. D. Schotten, G. Fettweis, and S. Stańczak, “Berlin V2X: A machine learning dataset from multiple vehicles and radio access technologies,” in *Proc. IEEE Vehicular Technology Conference Spring*. Florence, Italy: IEEE, Apr. 2023, doi: 10.48550/arXiv.2212.10343.

[7] A. Narayanan, X. Zhang, R. Zhu, A. Hassan, S. Jin, X. Zhu, X. Zhang, D. Rybkin, Z. Yang, Z. M. Mao, F. Qian, and Z.-L. Zhang, “A variegated look at 5G in the wild: Performance, power, and QoE implications,” in *Proc. ACM SIGCOMM Conference*. Virtual: Association for Computing Machinery, Aug. 2021, doi: 10.1145/3452296.3472923.

[8] B. Sliwa, H. Schippers, and C. Wietfeld, “Machine learning-enabled data rate prediction for 5G NSA vehicle-to-cloud communications,” in *Proc. IEEE 5G World Forum*, Virtual, Oct. 2021, doi: 10.1109/5GWF52925.2021.00059.

[9] B. Sliwa and C. Wietfeld, “Empirical analysis of client-based network quality prediction in vehicular multi-MNO networks,” in *Proc. IEEE Vehicular Technology Conference Fall*. Honolulu, HI, USA: IEEE, Sep. 2019, doi: 10.1109/VTCFall.2019.8891392.

[10] S. Farthofer, M. Herlich, C. Maier, S. Pochaba, J. Lackner, and P. Dorfinger, “An open mobile communications drive test data set and its use for machine learning,” *IEEE Open Journal of the Communications Society*, vol. 3, pp. 1688–1701, Sep. 2022, doi: 10.1109/OJCOMS.2022.3210289.

[11] V. Raida, P. Svoboda, and M. Rupp, “Real world performance of LTE downlink in a static dense urban scenario - An open dataset,” in *Proc. IEEE Global Communications Conference*, Taipei, Taiwan, Dec. 2020, doi: 10.1109/GLOBECOM42002.2020.9348204.

[12] J. Thrane, D. Zibar, and H. L. Christiansen, “Model-aided deep learning method for path loss prediction in mobile communication systems at 2.6 GHz,” *IEEE Access*, vol. 8, pp. 7925–7936, Jan. 2020, doi: 10.1109/ACCESS.2020.2964103.

[13] K. Kousias, M. Rajiullah, G. Caso, U. Ali, O. Alay, A. Brunstrom, L. De Nardis, M. Neri, and M.-G. Di Benedetto, “A large-scale dataset of 4G, NB-IoT, and 5g non-standalone network measurements,” *IEEE Communications Magazine*, vol. 62, no. 5, pp. 44–49, May 2024, doi: 10.1109/MCOM.011.2200707.

[14] J. Thrane, D. Zibar, and H. L. Christiansen, “Comparison of empirical and ray-tracing models for mobile communication systems at 2.6 GHz,” in *Proc. IEEE Vehicular Technology Conference Fall*. Honolulu, HI, USA: IEEE, Sep. 2019, doi: 10.1109/VTCFall.2019.8891306.

[15] D. F. Kulzer, F. Debbichi, S. Stanczak, and M. Botsov, “On latency prediction with deep learning and passive probing at high mobility,” in *Proc. IEEE International Conference on Communications*. Montreal, QC, Canada: IEEE, Jun. 2021, doi: 10.1109/ICC42927.2021.9500495.

[16] G. Nikolov, M. Kuhn, A. McGibney, and B. L. Wenning, “ASR - Adaptive similarity-based regressor for uplink data rate estimation in

mobile networks," *IEEE Journal on Selected Areas in Communications*, vol. 38, no. 10, pp. 2284–2294, Oct. 2020, doi: 10.1109/JSAC.2020.3000414.

[17] A. Palaios, P. Geuer, J. Fink, D. F. Kulzer, F. Gottsch, M. Kasparick, D. Schaufele, R. Hernangomez, S. Partani, R. Sattiraju, A. Kumar, F. Burmeister, A. Weinand, C. Vielhaus, F. H. P. Fitzek, G. Fettweis, H. D. Schotten, and S. Stanczak, "Network under control: Multi-vehicle E2E measurements for AI-based QoS prediction," in *Proc. IEEE International Symposium on Personal, Indoor and Mobile Radio Communications*. Helsinki, Finland: IEEE, Sep. 2021, doi: 10.1109/PIMRC50174.2021.9569490.

[18] A. Palaios, C. L. Vielhaus, D. F. Külzer, C. Watermann, R. Hernangómez, S. Partani, P. Geuer, A. Krause, R. Sattiraju, M. Kasparick, G. P. Fettweis, F. H. P. Fitzek, H. D. Schotten, and S. Stańczak, "Machine Learning for QoS prediction in vehicular communication: Challenges and solution approaches," *IEEE Access*, vol. 11, pp. 92 459–92 477, Aug. 2023, doi: 10.1109/ACCESS.2023.3303528.

[19] Kaggle team, "Kaggle," https://www.kaggle.com.

[20] Papers with Code team, "Paperswithcode," https://paperswithcode.com.

[21] M. Peuster, S. Schneider, and H. Karl, "The softwarised network data zoo," in *Proc. International Conference on Network and Service Management*. IEEE, 2019, doi: 10.23919/CNSM46954.2019.9012740.

[22] U. Masood, H. Farooq, A. Imran, and A. Abu-Dayya, "Interpretable AI-based large-scale 3D pathloss prediction model for enabling emerging self-driving networks," *IEEE Transactions on Mobile Computing*, vol. 22, no. 7, pp. 3967–3984, Jul. 2023, doi: 10.1109/TMC.2022.3147191.

[23] CellMapper Serviced Limited, "CellMapper," https://www.cellmapper.net, 2024, (Accessed 2024.08.14).

[24] Opensignal Limited, "Opensignal," https://www.opensignal.com, 2024, (Accessed 2024.08.14).

[25] Zafaco GmbH, "Breitbandmessung," https://www.breitbandmessung.de/mobil-testen, 2024, (Accessed 2024.08.14).

[26] Federal Communications Commission, "FCC speed test," https://www.fcc.gov/BroadbandData/speed-test-app, 2021, (Accessed 2024.08.14).

[27] Y. Li, C. Peng, Z. Zhang, Z. Tan, H. Deng, J. Zhao, Q. Li, Y. Guo, K. Ling, B. Ding, H. Li, and S. Lu, "Experience: A five-year retrospective of MobileInsight," in *Proc. International Conference on Mobile Computing and Networking*. New Orleans, Louisiana, USA: ACM, Sep. 2021, doi: 10.1145/3447993.3448138.

[28] M. Mroček, "NetMonster," https://netmonster.app, (Accessed 2024.08.14).

[29] V. Sathya, M. I. Rochman, and M. Ghosh, "Measurement-based coexistence studies of LAA & Wi-Fi deployments in Chicago," *Wireless Communications 28*, vol. 28, no. 1, pp. 136–143, Feb. 2021, doi: 10.1109/MWC.001.2000205.

[30] Qtrun Technologies, "NetworkSignalGuru," https://www.qtrun.com/eng/nsg, 2022, (Accessed 2024.08.14).

[31] H. Schippers, "CNI-Cell-Tracker," https://github.com/hendrikschippers/CNI-Cell-Tracker, 2021.

[32] H. Schippers, S. Böcker, and C. Wietfeld, "Data-driven digital mobile network twin enabling mission-critical vehicular applications," in *Proc. IEEE Vehicular Technology Conference Spring*. Florence, Italy: IEEE, Jun. 2023.

[33] M. Mroček, "Netmonster-Core," https://github.com/mroczis/netmonster-core, Dec. 2022, release 1.2.0.

[34] F. Jomrich, A. Herzberger, T. Meuser, B. Richerzhagen, R. Steinmetz, and C. Wille, "Cellular bandwidth prediction for highly automated driving - evaluation of machine learning approaches based on real-world data," in *Proc. International Conference on Vehicle Technology and Intelligent Transport Systems*. Funchal, Madeira, Portugal: SciTePress, Mar. 2018, doi: 10.5220/0006692501210132.

[35] D. Raca, A. H. Zahran, C. J. Sreenan, R. K. Sinha, E. Halepovic, R. Jana, V. Gopalakrishnan, B. Bathula, and M. Varvello, "Empowering video players in cellular: Throughput prediction from radio network measurements," in *Proc. ACM Multimedia Systems Conference*, ser. MMSys '19. New York, USA: Association for Computing Machinery, Jun. 2019, doi: 10.1145/3304109.3306233.

[36] A. Samba, Y. Busnel, A. Blanc, P. Dooze, and G. Simon, "Instantaneous throughput prediction in cellular networks: Which information is needed?" in *Proc. IFIP/IEEE Symposium on Integrated Network and Service Management (IM)*. Lisbon, Portugal: IEEE, May 2017, doi: 10.23919/INM.2017.7987345.

[37] B. Sliwa, R. Falkenberg, T. Liebig, N. Piatkowski, and C. Wietfeld, "Boosting vehicle-to-cloud communication by machine learning-enabled context prediction," *IEEE Transactions on Intelligent Transportation Systems*, vol. 21, no. 8, pp. 3497–3512, Aug. 2020.

[38] C. Yue, R. Jin, K. Suh, Y. Qin, B. Wang, and W. Wei, "LinkForecast: Cellular link bandwidth prediction in LTE networks," *IEEE Transactions on Mobile Computing*, vol. 17, no. 7, pp. 1582–1594, Jul. 2018, doi: 10.1109/TMC.2017.2756937.

[39] A. Narayanan, E. Ramadan, J. Carpenter, Q. Liu, Y. Liu, F. Qian, and Z.-L. Zhang, "A first look at commercial 5G performance on smartphones," in *Proc. The Web Conference*, ser. WWW '20. New York, NY, USA: Association for Computing Machinery, Apr. 2020, doi: 10.1145/3366423.3380169.

[40] D. Minovski, N. Ögren, K. Mitra, and C. Åhlund, "Throughput prediction using machine learning in LTE and 5G networks," *IEEE Transactions on Mobile Computing*, vol. 22, no. 3, pp. 1825–1840, Mar. 2023, doi: 10.1109/TMC.2021.3099397.

[41] A. S. Khatouni, F. Soro, and D. Giordano, "A machine learning application for latency prediction in operational 4G networks," in *Proc. IFIP/IEEE Symposium on Integrated Network and Service Management (IM)*, Washington DC, USA, Apr. 2019.

[42] D. Raca, A. Zahran, C. Sreenan, R. Sinha, E. Halepovic, R. Jana, and V. Gopalakrishnan, "Back to the future: Throughput prediction for cellular networks using radio KPIs," in *Proc. ACM Workshop on Hot Topics in Wireless*. New York, USA: Association for Computing Machinery, Oct. 2017, doi: 10.1145/3127882.3127892.

[43] S. Barmpounakis, L. Magoula, N. Koursioumpas, R. Khalili, J. M. Perdomo, and R. P. Manjunath, "LSTM-based QoS prediction for 5G-enabled connected and automated mobility applications," in *Proc. IEEE 5G World Forum*. Montreal, QC, Canada: IEEE, Oct. 2021, doi: 10.1109/5GWF52925.2021.00083.

[44] J. Rischke, P. Sossalla, S. Itting, F. H. P. Fitzek, and M. Reisslein, "5G campus networks: A first measurement study," *IEEE Access*, vol. 9, pp. 121 786–121 803, Aug. 2021, doi: 10.1109/ACCESS.2021.3108423.

[45] S. Choi and C. Kim, "A study on latency prediction in 5G network," in *Proc. International Conference on Ubiquitous and Future Networks*. Paris, France: IEEE, Jul. 2023, doi: 10.1109/ICUFN57995.

2023.10199172.

[46] B. Sliwa, M. Geis, C. Bektas, M. López, P. Mogensen, and C. Wietfeld, "DRaGon: Mining latent radio channel information from geographical data leveraging deep learning," in *Proc. IEEE Wireless Communications and Networking Conference*. Austin, TX, USA: IEEE, Apr. 2022, doi: 10.1109/WCNC51071.2022.9771981.

[47] M. Geis, B. Sliwa, C. Bektas, and C. Wietfeld, "TinyDRaGon: Lightweight radio channel estimation for 6G pervasive intelligence," in *Proc. IEEE Future Networks World Forum*. Montreal, QC, Canada: IEEE, Oct. 2022, doi: 10.1109/FNWF55208.2022.00121.

[48] 3rd Generation Partnership Project (3GPP), "Physical layer measurements," Technical Specification (TS) 38.215, Jul. 2024, version 18.3.0.

[49] C. Johnson, *5G New Radio in Bullets*, 1st ed. Independently published, 2019.

[50] H. Schippers, S. Böcker, and C. Wietfeld, "System for continuous multi-dimensional mobile network KPI tracking and prediction in drifting environments," in *Proc. IEEE International Systems Conference*, Vancouver, Canada, 2023.

[51] 3rd Generation Partnership Project (3GPP), "Nq and Nq' application protocol (Nq-AP); Stage 3," Technical Specification (TS) 29.405, Apr. 2024, version 18.0.0.

[52] ——, "Evolved universal terrestrial radio access (E-UTRA); Physical channels and modulation," Technical Specification (TS) 36.211, Apr. 2024, version 18.0.1.

[53] City of Dortmund, "OpenData Dortmund," https://open-data.dortmund.de, (Accessed 2024.08.14).

[54] ——, "Statistikatlas - 2019," https://www.dortmund.de/dortmund/projekte/rathaus/verwaltung/dortmunder-statistik/downloads/215_-_statistikatlas_-_2019.pdf, Oct. 2019.

[55] H. Schippers, C. Schüler, B. Sliwa, and C. Wietfeld, "System modeling and performance evaluation of predictive QoS for future tele-operated driving," in *Proc. IEEE International Systems Conference*. Virtual: IEEE, Apr. 2022, doi: 10.1109/SysCon53536.2022.9773810.

[56] V. Raida, P. Svoboda, M. Koglbauer, and M. Rupp, "On the stability of RSRP and variability of other KPIs in LTE downlink - An open dataset," in *Proc. IEEE Global Communications Conference*, Taipei, Taiwan, Dec. 2020, doi: 10.1109/GLOBECOM42002.2020.9348145.

[57] P. Jörke and C. Wietfeld, "How green networking may harm your IoT network: Impact of transmit power reduction at night on NB-IoT performance," in *Proc. IEEE World Forum on Internet of Things*. New Orleans, LA, USA: IEEE, Jun. 2021, doi: 10.5220/0006692501210132.

[58] F. Pedregosa, G. Varoquaux, A. Gramfort, V. Michel, B. Thirion, O. Grisel, M. Blondel, P. Prettenhofer, R. Weiss, V. Dubourg, J. Vanderplas, A. Passos, D. Cournapeau, M. Brucher, M. Perrot, and E. Duchesnay, "Scikit-Learn: Machine learning in Python," *Journal of Machine Learning Research*, vol. 12, pp. 2825–2830, Nov. 2011, doi: 10.5555/1953048.2078195.

[59] S. M. Lundberg and S.-I. Lee, "A unified approach to interpreting model predictions," in *Proc. International Conference on Neural Information Processing Systems*. Red Hook, NY, USA: Curran Associates Inc., 2017.

[60] H. Schippers and C. Wietfeld, "Data-driven energy profiling for resource-efficient 5G vertical services," in *Proc. IEEE Consumer Communications & Networking Conference*. Las Vegas, USA: IEEE, Jan. 2024, doi: 10.1109/CCNC51664.2024.10454791.

Authors

Hendrik Schippers (Student Member, IEEE) received the M.S. degree in electrical engineering and information technology from TU Dortmund University, Dortmund, Germany, in 2021. He is currently a research assistant at the Communication Networks Institute (CNI), Faculty of Electrical Engineering and Information Technology, TU Dortmund University. His research interests cover cellular 5G and beyond networks, focusing on the reliable prediction of connectivity quality for resource- and energy-efficient communication.

Melina Geis (Student Member, IEEE) received the M.S. degree in electrical engineering and information technology from TU Dortmund University, Dortmund, Germany, in 2021. She is currently a research assistant at the Communication Networks Institute (CNI), Faculty of Electrical Engineering and Information Technology, TU Dortmund University. Her research interests cover the useful application of machine learning in 6G and beyond networks focusing on radio propagation modeling and network planning.

Stefan Böcker (Member, IEEE) received his Dipl.-Ing. degree from TU Dortmund University, Dortmund, Germany, in 2013. He started as a research assistant at the Communication Networks Institute (CNI), Faculty of Electrical Engineering and Information Technology, TU Dortmund University. In 2016, he took over as the institute's head of the research group for 5G networks before being appointed chief engineer in 2021, where he is currently responsible for the coordination of third-party-funded research activities. His main research interests are scalability in unlicensed frequency domains, 5G networks with a focus on mMTC, as well as operation of private networks in licensed domains, with a special interest in industrial IoT environments.

Christian Wietfeld (Senior Member, IEEE) received the Dr.-Ing. and Dipl.-Ing. degrees from RWTH Aachen University, Aachen, Germany. He is currently a Full Professor and the Head of the Communication Networks Institute at TU Dortmund University, Dortmund, Germany. For more than 30 years, he has been a Coordinator of and a Contributor to large-scale research projects on Internet-based mobile communication systems within both academia and industry at RWTH Aachen (1992–1997), Siemens AG (1997–2005), and TU Dortmund (2005 to date). His current research interests include the design and performance evaluation of 5G and 6G communication networks for cyber-physical systems in energy, transport, robotics, and emergency response. Prof. Wietfeld is the author of more than 300 peer-reviewed papers and holds several patents. He has been a co-founder of the IEEE Global Communications Conference Workshop on Wireless Networking for Unmanned Autonomous Vehicles and is a member of the Technical Editor Board of the IEEE Wireless Communication Magazine. In addition to more than 15 IEEE Best Paper Awards, he received the ITU-T Outstanding Contribution Award for his work on the standardization of next-generation mobile network architectures.